

1 **Consumption of atmospheric methane by the Qinghai–Tibetan**  
2 **Plateau alpine steppe ecosystem**

3 **Hanbo Yun<sup>1,2,3</sup>, Qingbai Wu<sup>1\*</sup>, Qianlai Zhuang<sup>3\*</sup>, Anping Chen<sup>4\*</sup> Tong Yu<sup>3</sup>, Zhou**  
4 **Lyu<sup>3</sup>, Yuzhong Yang<sup>1</sup>, Huijun Jin<sup>1</sup>, Guojun Liu<sup>1</sup>, Yang Qu<sup>3</sup>, Licheng Liu<sup>3</sup>**

5  
6 **1. State Key Laboratory of Frozen Soil Engineering, Northwest Institute of Eco–**  
7 **Environment and Resources, Chinese Academy of Sciences, Lanzhou, Gansu 730000,**  
8 **China**

9 **2. Key Laboratory for Land Surface Process and Climate Change in Cold and Arid**  
10 **Regions, Chinese Academy of Sciences, Lanzhou, 730000, China**

11 **3. Department of Earth, Atmospheric, and Planetary Sciences, Purdue University, West**  
12 **Lafayette, Indiana 47907, USA**

13 **4. Department of Forestry and Natural Resources, Purdue University, West Lafayette,**  
14 **Indiana 47907, USA**

15  
16 **\*Authors for correspondence: [qbwu@lzb.ac.cn](mailto:qbwu@lzb.ac.cn) [Q. W.], [qzhuang@purdue.edu](mailto:qzhuang@purdue.edu) [Q.Z.],**

17 **[apchen1111@gmail.com](mailto:apchen1111@gmail.com) [A.C.]**

18

19

20

A manuscript for *The Cryosphere*

21

22

May 30, 2018

23 **Abstract**

24 The Methane (CH<sub>4</sub>) cycle on the Qinghai–Tibetan Plateau (QTP), the world’s largest high–  
25 elevation permafrost region, is sensitive to climate change and subsequent freezing and thawing  
26 dynamics. Yet, its magnitudes, patterns, and environmental controls are still poorly understood.  
27 Here, we report results from five continuous year–round CH<sub>4</sub> observations from a typical alpine  
28 steppe ecosystem in the QTP permafrost region. Our results suggest that the QTP permafrost  
29 region was a CH<sub>4</sub> sink of  $-0.86 \pm 0.23$  g CH<sub>4</sub>–C m<sup>-2</sup> yr<sup>-1</sup> over 2012 – 2016, a rate higher than that  
30 of many other permafrost areas, such as the Arctic tundra in northern Greenland, Alaska, and  
31 western Siberia. Soil temperature and soil water content were dominant factors controlling CH<sub>4</sub>  
32 fluxes, however, their correlations changed with soil depths, due to freezing and thawing  
33 dynamics. This region was a net CH<sub>4</sub> sink in autumn, but a net source in spring, despite both  
34 seasons experiencing similar top soil thawing and freezing dynamics. The opposite CH<sub>4</sub>  
35 source/sink function in spring versus in autumn was likely caused by the respective seasons  
36 specialized freezing and thawing processes, which modified the vertical distribution of soil  
37 layers that are highly mixed in autumn, but not in spring. Furthermore, the traditional definition  
38 of four seasons failed to capture the pattern of the annual CH<sub>4</sub> cycle. We developed a new  
39 seasonal division method based on soil temperature, bacterial activity, and permafrost active  
40 layer thickness, which significantly improved the modelling of the annual CH<sub>4</sub> cycle.  
41 Collectively, our findings highlight the critical role of fine–scale climate freezing and thawing  
42 dynamics in driving permafrost CH<sub>4</sub> dynamics, which needs to be better monitored and modelled  
43 in Earth system models.

## 44 1. Introduction

45 Since 2007, the global atmospheric methane concentration [CH<sub>4</sub>] continues to rise, after  
46 remaining stable between the 1990s and 2006 (Rigby et al., 2008; IPCC, 2013; Patra and Kort,  
47 2016). Understanding mechanisms for this recent increase requires improved knowledge on  
48 methane (CH<sub>4</sub>) sources and sinks for regional and global CH<sub>4</sub> budgets (Kirschke et al., 2013;  
49 Zona et al., 2016). However, estimates on global CH<sub>4</sub> emissions and consumptions are still  
50 highly uncertain (Spahni et al., 2011; Kirschke, 2013). In particular, the bottom–up approach,  
51 which estimates CH<sub>4</sub> budgets using ground observations and inventory, overestimated the global  
52 CH<sub>4</sub> budget by 6~20 times, compared to the atmospherically constrained top–down approach  
53 (Zhu et al., 2004; Lau et al., 2015). This discrepancy is partly due to limited monitoring data and  
54 to our poor understanding of important factors regulating the production and consumption of  
55 CH<sub>4</sub> ( Whalen and Reeburgh, 1990; Dengel et al., 2013; Bohn et al., 2015).

56 The Qinghai–Tibetan Plateau (QTP) is the world’s largest high–elevation permafrost  
57 region of  $1.23 \times 10^6$  km<sup>2</sup> (Wang et al., 2000). The QTP is currently experiencing a rapid change  
58 in climate, which affects freezing and thawing processes. The change in the freezing and thawing  
59 dynamic profoundly impacts methanotrophy and methanogenesis, which consequently impacts  
60 net CH<sub>4</sub> fluxes (Mastepanov *et al.*, 2013; Lau et al., 2015). However, due to the scarcity of high  
61 temporal–resolution year–round environment and CH<sub>4</sub> monitoring, we still know little about the  
62 size, seasonal pattern, and underlying controls of climate and permafrost freezing and thawing,  
63 and the resulting effects on CH<sub>4</sub> exchanges in the QTP permafrost region (Cao et al., 2008; Wei  
64 et al., 2015a; Song et al., 2015; ). This knowledge gap also hampers our capacity to predict and  
65 understand QTP permafrost CH<sub>4</sub> cycles under current and projected future climates.

66 Here, we report results from a 5-year continuous *in situ* monitoring of CH<sub>4</sub> dynamics  
67 with an eddy covariance (EC) technique at the Beilu'he Research Station, which is a  
68 representative site for QTP permafrost heartland. The site was covered by alpine steppe  
69 vegetation from January 1<sup>st</sup>, 2012 to December 31<sup>st</sup>, 2016. The primary aims of this investigation  
70 are to understand (1) the long-term annual and seasonal variation of the methane budget for a  
71 typical alpine permafrost site in the QTP, and (2) the environmental factors controlling these  
72 CH<sub>4</sub> variations and possible underlying mechanisms. In addition, while the consumption and  
73 production of ecosystem methane are known through microbial activities, conventional  
74 investigations on seasonal methane fluxes usually used climate or vegetation defined "seasons".  
75 Therefore, a third research goal of this current study is to investigate if the classical vegetation  
76 productivity-based definition of growing season will be useful for defining the methane flux  
77 seasonality.

78 There are three advantages of our data acquisition system. First, the EC system recorded  
79 the data of CH<sub>4</sub> fluxes, climate, and soil properties every half hour. As the QTP permafrost is  
80 characterized by a rapidly changing climate and a rapidly changing soil freezing and thawing  
81 dynamic, even over a time period as short as one day, different aerobic or anaerobic soil  
82 environments that favor different types of CH<sub>4</sub> bacteria may change (Rivkina et al., 2004; Lau et  
83 al., 2015). Thus, high-resolution *in situ* monitoring data enables us to quantify CH<sub>4</sub> exchange  
84 patterns from diel to annual time-scales and investigate their major environmental drivers.  
85 Second, our field investigation spanned five full calendar years, including both plant growing  
86 and non-growing seasons. Observations of the plant non-growing season, which accounts for  
87 two-thirds of a year, were very rare in current literature (Song et al., 2015). Third, the EC system  
88 we used overcame some technical problems caused by the often used static chambers, including

89 limited representation of local site heterogeneity and additional heating of the soil surface  
90 (Chang et al., 2014; Wei et al., 2015b).

## 91 **2. Methods**

### 92 **2.1 Site Description**

93 The research site, Beilu'he permafrost research station (34° 09' 006" N, 92° 02' 080" E),  
94 is located in the alpine steppe continuous permafrost area of the northern QTP, about 320  
95 kilometers southwest of Golmud, Qinghai Province (Figure 1). At an elevation of 4765 meters,  
96 the air is thin with only 0.6 standard atmospheric pressure. According to *in situ* observations, the  
97 site receives solar radiation of about 6720 MJ meter<sup>-2</sup>. The non-growing season is long and cold,  
98 with 225 days per year having an annual air temperature of -18 °C on average from 2012 to  
99 2016. The site's growing season is short and cool, with 140 days per year from 2012 to 2016,  
100 and a mean annual air temperature of 4.6 °C. According to the site drilling exploration, the  
101 permafrost depth can extend to 50 – 70 m below ground, and the thickness of the active layer  
102 (ALT) is about 2.2 – 4.8 m. The soil is composed of Quaternary fine sand or silt (Table 1),  
103 overlying on Triassic mudstone or weathered marl. Dominant plant species include: *Carex*  
104 *moorcroftii* Falc. ex Boott, *Kobresia tibetica* Maxim, *Androsace tanggulashanensis*, and  
105 *Rhodiola tibetica*. Vegetation coverage is approximately 33.5% and the average plant height is  
106 15 cm.

### 107 **2.2 Eddy Covariance observations**

108 We have continuously monitored CH<sub>4</sub>, carbon dioxide (CO<sub>2</sub>), water (H<sub>2</sub>O), and heat flux  
109 using a standard eddy covariance system tower 3 meters above the ground. CH<sub>4</sub> flux was measured  
110 with an open-path CH<sub>4</sub> analyzer system (Figure 1:d; LI-7700, LI-COR Inc., Lincoln, NE, USA).

111 The precision is 5 ppb, with RMS noise at 10 Hz and 2000 ppb. The instrument was placed on site  
112 on August 8<sup>th</sup>, 2011, and then connected to a three-dimensional sonic anemometer (heat and water  
113 flux; CSAT3, Campbell Scientific, and Logan, UT, USA; precision is 0.1 °C; accuracy is within  
114 1% of reading for half-hour) and an open-path infrared gas analyzer (CO<sub>2</sub> flux; LI-7500A, LI-  
115 COR Inc., Lincoln, NE, USA; the precision is 0.01 μmol m<sup>-2</sup> s<sup>-1</sup> and the accuracy is within 1% of  
116 reading for half-hour, zero drift per °C is ± 0.1 ppm typical) on January 1<sup>st</sup>, 2012, when the system  
117 worked steadily. Monitoring data was recorded and stored at 10 Hz using a data logger (LI-7550,  
118 LI-COR Inc., Lincoln, NE, USA).

119 The operation, calibrations, and maintenance of the EC system followed standard  
120 procedures. To reduce the LI-7500A surface heating/cooling influence on CO<sub>2</sub> and H<sub>2</sub>O molar  
121 densities in tough environments, each year “summer style” was used in Li-7500A, in which  
122 surface temperature setting is 5 °C during May 1<sup>st</sup> to September 30<sup>th</sup>. “Winter style” was used from  
123 October 1<sup>st</sup> to the next year April 30<sup>th</sup> in Li-7500A, in which surface temperature setting is -5 °C.  
124 Calibrations of CO<sub>2</sub>, water vapor, and dew point generator measurements for LI-7500A analyzers  
125 were performed regularly by the China Land-Atmosphere Coordinated Observation System  
126 (CLAROS). Up-and-down mirrors of LI-COR 7700 were cleaned regularly every 30 days to  
127 make sure the signal strength was stronger than 80. All of these instruments were powered by  
128 solar-panel and battery.

### 129 **2.3 Micrometeorological and Soil Measurements**


130 A wide range of meteorological variables were measured by a standard automatic  
131 meteorological tower 3 meters above the ground and 5 meters north of the eddy covariance  
132 tower. Net radiation (R<sub>n</sub>) and albedo were measured with a four-component radiometer (R<sub>n</sub>;  
133 CNR-1, Kipp and Zonen, the Netherlands). Air temperature (T<sub>air</sub>), air relative humidity, and


134 atmospheric pressure were measured with a temperature and humidity sensor (HMP45C, Vaisala  
135 Inc., Helsinki, Finland) in the meteorological tower. A rain gauge (TE525MM, Texas Electronics  
136 Inc., Dallas, TX, USA) was used to measure the precipitation process. Wind speed and wind  
137 direction were observed using a propeller anemometer placed on the top of the meteorological  
138 tower.

139 We also measured soil heat fluxes, soil temperature and soil relative water content (SWC).  
140 In August 2010, we installed soil environmental sensors 10 meters from the eddy covariance  
141 tower for soil sample collection. Two self-calibrating soil heat flux (SHF) sensors (HFP01) were  
142 placed 5 cm and 15 cm below the ground. A group pF-Meter sensor (GEO-Precision, Germany)  
143 was embedded in the soil under the meteorological tower to measure soil temperature ( $T_{\text{soil}}$ ) at 0  
144 cm, 5 cm, 10 cm, 15 cm, 20 cm, 30 cm, 40 cm, 50 cm, 70 cm, 80 cm, 100 cm, 150 cm, 160 cm,  
145 and 200 cm depth. The pF meter sensors also measured SWC at 10 cm, 20 cm, 40 cm, 80 cm,  
146 and 160cm depth.

147 All of above environmental parameters were synchronously monitored with eddy  
148 covariance, and the data was recorded every 30 minutes by CR3000 (Data logger, Campbell Data  
149 Taker Ltd, Salt Lake City, UT, USA). The air temperature sensors, the humidity sensors, and the  
150 pF meter sensors were calibrated in the State Key Laboratory of Frozen Soil Engineering at the  
151 Chinese Academy of Sciences in order to ensure the measurement accuracy was within  $\pm 0.05$  °C  
152 and  $\pm 5\%$ , respectively.

153 We also sampled soil profiles for soil physical and chemical measurements with one 1  
154 meter  $\times$  1 meter  $\times$  2 meter pit 10 meter from the eddy covariance tower in August 2010. Five  
155 profile samples were taken from the pit at depths 0 – 20 cm, 20 – 50 cm, 50 – 120 cm, 120 –

156 160 cm, and 160 – 200 cm. Every depth was ated five times after being fully mixed. Then  
157 each depth was stored in soil sample aluminum boxes and carefully sealed to prevent gas  
158 exchanges with air. The clod method was used to investigate the field wet bulk density (weight  
159 of soil per unit volume; Cate and ~~re~~ Nelson, 1971). The soil moisture content was calculated  
160 gravimetrically by the ratio of the mass of water present to the oven-dry (60 °C for 24 hour)  
161 weight of the soil sample. The soil organic carbon (SOC) content of the air-dried soil samples  
162 was analyzed using the wet combustion method, Walkley–Black modified acid dichromate  
163 digestion, FeSO<sub>4</sub> titration, and an automatic titrator. Total nitrogen (TN) and pH were measured  
164 using standard soil test procedures from the Chinese Ecosystem Research Network.

165 To understand the potential effect of soil thawing and freezing dynamics on CH<sub>4</sub> fluxes,  
166 we also reconstructed and verified semi-monthly data of soil active layer thickness (ALT).  
167 Following Muller’s original definition, ALT is the maximum thaw depth in the late autumn using  
168 a linear interpolation of  T<sub>soil</sub> profiles between two neighboring points above and below the 0 °C  
169 isotherm (Muller, 1947). We used records of the soil thawing thickness measured with a self-  
170 made geological probe to verify the ALT data semi-monthly. More information about the  
171 measurement procedure was previously described by Wu and Zhang (2010a).

## 172 **2.4 Microbial Activity**

173 To understand how soil microbial activity may have impacted the CH<sub>4</sub> fluxes, we sampled  
174 100-gram soils for soil microbial activity measurements. These soils were obtained using a soil  
175 sample drill device (Ø=0.03 m), with depths of 0 – 25 cm taken every 5 days within 100 m of the  
176 eddy covariance tower. The sampled soil was fully mixed and divided into two equal parts. Each  
177 part was then stored in sterilized aluminum boxes and then placed in liquid nitrogen, before  
178 sending to the lab for microbe RNA extraction. We then used a real-time PCR method to



179 genetically test methanotrophic / archaeal methanogens, and the procedure was repeated three  
180 times for each sample. By setting the maximum methanotrophic / archaeal methanogens gene  
181 expression cyclic number as 1, we calculated the variety coefficient of methanotrophic and  
182 archaeal methanogens gene expressions ( $\Delta I$  and  $\Delta II$ , respectively; %) with equation (1):

$$183 \quad \Delta_i = \frac{x_i}{X_{Max}} \quad \dots \quad (1)$$

184  $\Delta_i$  is for the  $i^{\text{th}}$  methanotrophic/archaeal methanogens gene expression;  $x_i$  is the  
185 methanotrophic / archaeal methanogen gene expression cyclic number of the  $i^{\text{th}}$  time;  $X_{Max}$  is the  
186 maximum methanotrophic / archaeal methanogen gene expression cyclic number of the soil  
187 group from 2012 to 2016.

## 188 **2.5 EC Data Processing and Data Filtering**

189 Data collected from January 1<sup>st</sup>, 2012 to December 31<sup>st</sup>, 2016 was used in this study. Before  
190 processing, we removed data that was recorded at the time of precipitation events or with LI-7700  
191 signal strength under 85. We first processed the raw data in Eddypro 6.2.0 (LI-COR, Lincoln, NE,  
192 USA). We adopted standardized procedures recommended in Lee et al. (2006) to process half-  
193 hourly flux raw measurements to ensure their quality.

194 1) Data was processed through statistical analysis in Eddypro 6.2.0 including: spike  
195 removal (accepted spikes < 5% and replaced spikes with linear interpolation), amplitude resolution  
196 (range of variation:  $7.0 \sigma$ , number of bins: 100, accepted empty bins: 70%), drop-outs (percentile  
197 defining extreme bins: 10, accepted central drop-outs: 10%, accepted extreme drop-outs: 6%),  
198 absolute limits ( $-30 \text{ m s}^{-1} < U < 30 \text{ m s}^{-1}$ ,  $-5 \text{ m s}^{-1} < W < 5 \text{ m s}^{-1}$ ,  $-40 \text{ }^\circ\text{C} < T_s < 40 \text{ }^\circ\text{C}$ ,  $200 \text{ } \mu\text{mol}$

199 mol<sup>-1</sup> < CO<sub>2</sub> < 500 μmol mol<sup>-1</sup>, 0 μmol mol<sup>-1</sup> < H<sub>2</sub>O < 40 μmol mol<sup>-1</sup>, 0.17 μmol < CH<sub>4</sub> < 1000  
200 μmol), Skewness and kurtosis (-2.0 < Skewness lower limit < -1.0, 1.0 < Skewness up limit < 2.0;  
201 1.0 < Kurtosis lower limit < 2.0, 5.0 < Kurtosis upper limit < 8.0), discontinuities (hard-flag  
202 threshold: U = 4.0, W = 2.0, T<sub>S</sub> = 4.0, CO<sub>2</sub> = 40, CH<sub>4</sub> = 40, and H<sub>2</sub>O = 3.26; soft-flag threshold: U  
203 = 2.7, W = 1.3, T<sub>S</sub> = 2.7, CO<sub>2</sub> = 27, CH<sub>4</sub> = 30, and H<sub>2</sub>O = 2.2), angle of attack (minimum angle of  
204 attack = -30, maximum angle attack = 30, accepted amount of outliers = 10%), and steadiness of  
205 horizontal wind (accepted wind relative instationarity = 0.5) (Vickers and Mahrt, 1997; Mauder et  
206 al., 2013).

207 2) The data was then corrected using atmosphere physical calculations expressed by: axis  
208 rotations of tilt correction (double rotation), time lags compensation (covariance maximization),  
209 and compensating density fluctuations of Webb–Pearman–Leuning (WPL) terms. When CO<sub>2</sub> and  
210 H<sub>2</sub>O molar densities are measured with the LI-COR 7500 / LI-COR 7500A in cold environments  
211 (low temperatures below -10 °C), a correction should be applied to account for the additional  
212 instrument–related sensible heat flux, due to instrument surface heating / cooling. Thus, we  
213 implemented the correction according to Burba et al. (2008), which involves calculating a  
214 corrected sensible heat flux ( $H'$ ) by adding estimated sensible heat fluxes from key instrument  
215 surface elements, including the bottom window ( $H_{bot}$ ), top window ( $H_{top}$ ), and spar ( $H_{spar}$ ) to the  
216 ambient sensible heat flux ( $H$ ):

$$217 \quad H' = H + H_{bot} + H_{top} + 0.15 \times H_{spar} \quad (2)$$

218 3) Quality assurance (QA) / quality control (QC) were ensured through spectral analysis  
219 and corrections analysis in Eddypro 6.2.0. Spectra and co-spectra calculations used power-of-two  
220 samples to speed up the Fast Fourier Transform (FFT) algorithm. Spectra and co-spectra QA / QC

221 by filter were made according to Vickers and Mahrt (1997) test results, and Mauder and Foken  
222 (2004) micrometeorological quality test results. Low-frequency range spectral correction was  
223 done considering high-pass filtering effects. High-frequency range spectral correction was done  
224 considering low-pass filtering effects (Moncrieff et al., 2004).

225 4) We chose values “0”, “1”, “2” to flag the processed flux data into three quality classes in  
226 Eddypro 6.2.0. The combined flag attains the value “0” for best quality fluxes, “1” for fluxes  
227 suitable for general analysis, such as annual budgets, and “2” for fluxes that should be discarded  
228 from the results dataset. For our dataset, approximately 67% of the data fell into Class 0, 12% in  
229 Class 1, and 21% in Class 2.

230 5) Our analysis indicated that, under average meteorological conditions, 80% of the flux  
231 (footprint) came from an area within 175 m of the eddy covariance tower.


232 In addition, we also adopted the method in Burba et al. (2008) to adjust the half-hour flux  
233 data, to avoid apparent measuring errors. In doing this, we rejected half-hour flux data that fell  
234 into one of the following situations: (1) incomplete half-hour measurements, (2) measurements  
235 under rain impacts, (3) nighttime measurements under stable atmospheric conditions ( $U^*$ , friction  
236 velocity,  $\leq 0.1 \text{ m s}^{-1}$ ), and (4) abnormal values detected by a three-dimensional ultrasonic  
237 anemometer. This screening resulted in the rejection of about 20.7% of the flux data.

238 After the above data quality control, there was a 28.7% data gap for CH<sub>4</sub> fluxes over the  
239 entire examination period. These data gaps were then filled according to the method described in  
240 literature (Falge et al., 2001; Papale et al., 2003). We used a linear interpolation to fill the gaps if  
241 they were less than 2 hours, a method described in Falge *et al.* (2001) to fill gaps greater than 2  
242 hours, but less than 1 day, and an artificial neural network approach as described in Papale et al.

243 (2003) and Dengel et al. (2013) to fill gaps greater than 1 day.

244 The quality of the dataset was evaluated using the equation of energy closure:

$$245 \quad EBR = \sum (H + \lambda E) / \sum (R_n - G - S) \quad \dots \quad 3$$

246 where the *EBR* is surface energy balance ratio; *H* is heat flux;  $\lambda E$  is latent heat; *R<sub>n</sub>* is net  
247 radiation; *G* is soil heat flux (SHF); and *S* is heat storage of the vegetation canopy. As vegetation  
248 coverage at this research site is sparse, *S* is ignored. From 2012 to 2016, the *EBR* average was  
249 larger than 67.5%. 

250 We analyzed two different major sources of CH<sub>4</sub> flux gap-filling uncertainty. The first kind  
251 of uncertainty came from U\* threshold estimate. Following Burba et al. (2008), we excluded the  
252 probably false low CH<sub>4</sub> flux at low U\*. However, it was difficult to determine the value for the  
253 U\* threshold. For instance, when choosing a lower U\* threshold, the associated lower flux would  
254 contribute to the gap filling and the annual gross (Loescher, et al., 2006). The variance from 5% to  
255 95% of the bootstrapped values provided an average of the uncertainties **caused by the U\* to filter**  
**256 out.** The second uncertainty source was due to insufficient power supply. In this research, all  
257 instrument power was supplied by solar. Extended periods of rainy, cloudy, and snowy weather,  
258 would cause the instrument to stop working due to an insufficient power supply. When we used  
259 the ~~method to fill the gap~~ mentioned above, it would cause the CH<sub>4</sub> to deviate from the true value.  
260 To our knowledge, the CH<sub>4</sub> flux data was largely uncertain under rainy conditions.

## 261 ~~2.6 Based on microbial activities classification system of the four seasons~~

262 We redefined the four seasons of spring~~,~~ summer~~,~~ autumn~~,~~ and winter~~,~~ and based the  
263 parameters of the new seasons ~~on microbial activities~~ (Figure 2), ALT variety coefficients (ALT

264 variety coefficient =  $(ALT_{i+1} - ALT_i) / ALT_{Max}$ , where  $ALT_{Max}$  is the maximum of ALT per  
265 year), and  $T_{soil}$ . Below, we describe the start date of each season (The end date of a season is the  
266 day immediately before the start of the next season).

267 Spring<sub>-</sub> starts at the first day of two consecutive observation periods fulfilling both (1)  $(\Delta II$   
268  $+ \Delta I) / 2 \geq 15\%$ , and (2) the ALT variety coefficient  $\geq 0.05$ .

269 Summer<sub>-</sub> starts on the first day of two consecutive observation periods when (1)  $(\Delta II + \Delta I)$   
270  $/ 2 \geq 45\%$ , (2) ALT variety coefficient  $\geq 0.35$ , and (3) five successive days with  $T_{soil}$  at 40 cm  
271 soil depth  $\geq 0^\circ C$ .

272 Autumn<sub>-</sub> starts on the first day of two consecutive observation periods when (1)  $(\Delta II + \Delta I) /$   
273  $2 \geq 55\%$ , (2) the ALT variety coefficient  $\geq 0.60$ , and (3) five successive days the  $T_{soil}$  of 10  
274 cm  $< 5^\circ C$ .

275 Winter<sub>-</sub> starts on the first day of two consecutive observation periods that (1)  $(\Delta II + \Delta I) / 2$   
276  $< 15\%$  and the ALT variety coefficient  $< 0.05$ .

277 To test the robustness of our new seasonal division method in our methane cycle analysis,  
278 we compared empirical  $CH_4$  flux estimates using different season definitions (Table 2). In  
279 addition to our new method that was based on top soil microbe activity,  $T_{soil}$  of 0 – 40 cm, and  
280 permafrost active layer variability (hereafter refer to as SMT), we also used three conventional  
281 methods~~—one~~ based on ~~vegetation cover and temperature change (VCT), one~~ on Julian months  
282 (JMC), and ~~the other one~~ on vegetation phenology change (VPC). Specifically~~—~~ the VCT method  
283 splits a year into a plant growing season and a non-growing season; the JMC method assumes  
284 May to October as a plant growing season, and November to the following April as a non-

285 growing season; and the VPC method defines a plant growing season as the period between the  
286 time when all dominant grass species (*Carex Moorcroft Falc. ex Boott*, *Kobresia tibetica Maxim*,  
287 *Androsace tanggulashanensis*, *Rhodiola tibetica*) germinate and that when they all senesce.

## 288 **2.7 Statistical Analyses**

289 To understand the connections between CH<sub>4</sub> fluxes and associated environmental factors,  
290 we performed a series of statistical analyses, including correlation, principal component analyses  
291 (PCA), and linear regression analyses, in IBM SPSS (IBM SPSS Statistics 24; IBM, Armonk  
292 NY, USA). Specifically, we used bivariate correlation to examine pairwise relationships between  
293 environmental factors and CH<sub>4</sub> fluxes. We also used PCA and linear regressions to explore the  
294 sensitivity of CH<sub>4</sub> fluxes to simultaneous environmental fluctuations in wind speed, T<sub>air</sub>, air  
295 relative humidity, R<sub>n</sub>, vapor pressure deficit (VPD), albedo, SHF, SWC, and T<sub>soil</sub>. Before  
296 performing PCA and linear regressions, the entire dataset was examined for outliers (Cook's  
297 Distance, < 0.002), homogeneity of variance (Levene test,  $p < 0.05$ ), normality (Kolmogorov–  
298 Smirnov test, smooth line for histogram of Studentized residuals), collinearity (variance inflation  
299 factor,  $0 < \text{VIF} < 10$ ), potential interactions ( $t$ -test,  $p < 0.05$ ), and independence of observations  
300 ( $t$ -test,  $p < 0.05$ ).

301 We performed structural equation modeling (SEM) to evaluate the effects of  
302 environmental variables on CH<sub>4</sub> fluxes for different seasons. SEM is a widely-used multivariate  
303 statistical tool that incorporates factor analysis, path analysis, and maximum likelihood analysis.  
304 This method uses *priori* knowledge of the relationships between focus variables to verify the  
305 validity of hypotheses. Here we performed SEM analyses with AMOS 21.0 (Amos Development  
306 Corporation, Chicago, IL, USA). All data are presented as mean values with standard  
307 deviations.

### 308 3. Results

#### 309 3.1 Meteorological Conditions

310 We first reported the statistics of ~~environmental factors~~ at the Beilu'he Permafrost Weather  
311 Station ~~based on meteorological records from~~ 2012 to 2016. Mean annual Tair was -4.5 °C  
312 (Supplementary Figure 1), with minimum and maximum mean ~~dier~~ temperatures of -21.6 °C (12<sup>th</sup>  
313 January, 2012) and 13.8 °C (28<sup>th</sup> July, 2015), respectively. Average net radiation was 82.8 Wm<sup>-2</sup>,  
314 ~~while the maximum was~~ in August (136.2 Wm<sup>-2</sup>; Supplementary Figure 2). The average VPD was  
315 about 0.3, ~~while the maximum was~~ 0.98, and ~~the minimum was~~ 0.02 (Supplementary Figure 3).  
316 Mean annual precipitation was 335.4 mm (Figure 3), which was primarily based on rain and  
317 snowfall (only occupied 7%). ~~From 2012 to 2016, the maximum~~ precipitation was 2013 (488.3  
318 mm), and ~~the minimum was in~~ 2015 (310.0 mm). The majority of precipitation, approximately  
319 92%, occurred in the summer. During the winter, precipitation was rare and the mean value was  
320 about 6.7 mm, with the **value decreasing even further from 14.2 mm in 2012, to 2.1 mm in 2016.**  
321 Spring was another important rainfall period besides summer, with mean precipitation being about  
322 37.5 mm, or 8~17% of the total.

323 The Beilu'he site is windy during most of the year (Supplementary Figure 4). Its annual  
324 average speed was 4.4 m s<sup>-1</sup> from 2012 to 2016, **while its maximum and minimum wind speeds**  
325 **were 14.6 m s<sup>-1</sup> on 14<sup>th</sup> February, 2016 and 1.3 m s<sup>-1</sup> on 1<sup>st</sup> November, 2013, respectively.** Its winter,  
326 **spring, and autumn average wind speed were 5.4 m s<sup>-1</sup>, 4.3 m s<sup>-1</sup>, and 3.7 m s<sup>-1</sup>, respectively,** while  
327 the principal direction of the strongest winds were from the southwest. Late autumn, winter, and  
328 early spring drought brought increased risks of dust blowing days, with an average of 122 days  
329 within a year. Its summer average wind speed was about 3.30 m s<sup>-1</sup>, predominantly driven by the

330 southwest wind.

331 The SWC and Tsoil varieties of soil layers from 2012 to 2016 at the field site were  
332 summarized in Supplementary Figure 5 and Supplementary Figure 6, respectively. Mean SWC of  
333 depths 10 cm, 20 cm, 40 cm, 80 cm, and 160 cm were 14%, 9%, 8%, 14%, and 19%, respectively.  
334 Tsoil of depths 0 cm, 5 cm, 10 cm, 20 cm, 30 cm, 40 cm, 50 cm, 70 cm, and 80 cm corresponded  
335 with the Tair changes, but at depths 100 cm, 150 cm, 160 cm, and 200 cm did not correspond. The  
336 Tsoil of depth 200 cm had a remarkable difference from the Tsoil of other layers. The reason could  
337 be that peat existed in this layer, and that, during winter, the peat layer was not completely frozen.  
338 Supplementary Figure 7 shows SHF half-hour and diel scale varieties of 5 cm and 15 cm depth.  
339 The annual mean value of SHF at 5 cm and 15 cm depth is  $7.6 \text{ Wm}^{-2}$  and  $6.8 \text{ Wm}^{-2}$ , respectively.

340 Finally, we also reported the site's average soil freezing and thawing dynamics observed  
341 from January 2012 to December 2016 in Supplementary Figure 8. The duration of the active layer  
342 in the thawing state at 40 cm depth ranged from 174 to 188 days, with an average variation of up  
343 to 14 days. The average ALT is 4.4 m from 2012 to 2016.

### 344 **3.2 Annual, Seasonal and Diel Variabilities of Methane Fluxes**

345 Our results indicated that the Beilu'he site was a  $\text{CH}_4$  sink, with an annual mean strength  
346 of  $-0.86 \pm 0.23 \text{ g CH}_4\text{-C m}^{-2}$  (95% confidence interval; negative values mean  $\text{CH}_4$  sinks, positive  
347 values mean  $\text{CH}_4$  sources). The strength of the  $\text{CH}_4$  sink varies across different years from  $-0.57$   
348  $\pm 0.27 \text{ g CH}_4\text{-C m}^{-2} \text{ yr}^{-1}$  in 2015, to  $-1.49 \pm 0.38 \text{ g CH}_4\text{-C m}^{-2} \text{ yr}^{-1}$  in 2014 (Figure 3). The amount  
349 of gene expression by methanogens and methanotrophs at 0 – 25 cm soils in March and  
350 November, for instance, were about 16.8% and 35.6%, respectively, suggesting strong microbial  
351 activities even during the cold and dry plant non-growing season (Figure 2).



352 We also clearly observed CH<sub>4</sub> seasonal variations (Supplementary Figure 9) in both the  
353 amount of CH<sub>4</sub> exchanges and their diel cycles (Figure 4). In winter<sub>=</sub>, the net CH<sub>4</sub> flux at the  
354 Beilu'he site was an atmospheric source, with an average annual rate of  $0.41 \pm 0.16 \text{ g CH}_4\text{-C m}^{-2}$   
355  $\text{yr}^{-1}$  or  $4.35 \pm 0.33 \text{ mg CH}_4\text{-C m}^{-2} \text{ d}^{-1}$  (Supplementary Figure 9:a). It should also be noted that  
356 since the investigation started January 1<sup>st</sup>, 2012, and ended on December 31<sup>st</sup>, 2016, the 2011 ~  
357 2012 and 2016 ~ 2017 winters<sub>=</sub> were only about half of the regular length. The diel CH<sub>4</sub> cycle  
358 of an average winter<sub>=</sub> day was characterized by one single emission peak around 10:30am ~  
359 17:30 pm (Figure 4: a1, b1, c1, d1, e1 and f1).

360 In spring<sub>=</sub>, the Beilu'he site was a CH<sub>4</sub> source of  $0.90 \pm 0.37 \text{ g CH}_4\text{-C m}^{-2} \text{ yr}^{-1}$   
361 (Supplementary Figure 9:b), accounting for 53% of annual CH<sub>4</sub> emissions, or  $1.81 \pm 0.22 \text{ mg}$   
362  $\text{CH}_4\text{-C m}^{-2} \text{ d}^{-1}$ . For a typical spring<sub>=</sub> (Figure 4: a2, b2, c2, d2, and e2), diel CH<sub>4</sub> emission usually  
363 started at around 10:00 am ~ 10:30 am, when the thin ice layer on the soil surface started to  
364 thaw. It then reached the peak at 12:30 pm ~ 13:30 pm. The emission peak started to weaken at  
365 around 15:30 pm ~ 16:00 pm and reached around zero or even turned into a small sink after  
366 20:00 pm.

367 In summer<sub>=</sub>, the Beilu'he site was a CH<sub>4</sub> sink of  $-0.99 \pm 0.18 \text{ g CH}_4\text{-C m}^{-2} \text{ yr}^{-1}$   
368 (Supplementary Figure 9:c), or  $-13.28 \pm 0.38 \text{ mg CH}_4\text{-C m}^{-2} \text{ d}^{-1}$ . The diel cycle of CH<sub>4</sub> fluxes  
369 in summer<sub>=</sub> was characterized with two absorption peaks and one small emission peak (Figure 4:  
370 a3, b3, c3, d3, and e3). With T<sub>air</sub> increasing after sunrise, soils started to absorb atmospheric  
371 CH<sub>4</sub> and this soil uptake process reached its first peak at around 9:30 am ~ 10:30 am. After that,  
372 the continuously increasing T<sub>air</sub> turned to suppress CH<sub>4</sub> uptake and promote CH<sub>4</sub> emissions,  
373 likely due to different temperature sensitivities of methanotrophic and methanogenic bacteria. At

374 around 15:30pm ~ 16:00 pm, when  $T_{air}$  reached the maximum (Supplementary Figure 1-b),  
375  $CH_4$  emission also reached its peak. The following temperature decrease in the late afternoon  
376 again reversed the  $CH_4$  uptake / emission process, and by sunset we observed another  $CH_4$  sink  
377 peak. The rate of  $CH_4$  sink then decreased again through the night with further decreasing  
378 temperature.

379 Autumn<sub>–</sub> was another season with a net  $CH_4$  sink, with the season having the highest  
380 observed value for the site as a  $CH_4$  sink in 2013 (Supplementary Figure 9: d). The  $CH_4$  sink in  
381 autumn<sub>–</sub> varied between  $-0.69 \pm 0.19$  g  $CH_4-C$  m<sup>-2</sup> (2015), and  $-1.59 \pm 0.33$  g  $CH_4-C$  m<sup>-2</sup> (2013),  
382 with an average diel rate of  $-1.19 \pm 0.48$  g  $CH_4-C$  m<sup>-2</sup> yr<sup>-1</sup> or  $-13.31 \pm 0.28$  mg  $CH_4-C$  m<sup>-2</sup> d<sup>-1</sup>.  
383 The diel dynamics of autumn<sub>–</sub>  $CH_4$  fluxes was like a letter “V”, with a single sink peak during  
384 13:30 pm ~ 15:30 pm (Figure 4: a4, b4, c4, d4, and e4).

### 385 **3.3 Response of Methane Fluxes to Changes in Environmental Factors**

386 Diel fluxes of  $CH_4$  were highly correlated with many biotic and abiotic environmental  
387 factors, either positively or negatively (Table 3). Positive factors include metagenomics of both  
388 methanotrophic ( $r = 0.52$ ,  $p < 0.01$ ) and methanogens ( $r = 0.49$ ,  $p < 0.01$ ) at 0 – 25 cm soils,  
389 ALT ( $r = 0.43$ ,  $p < 0.01$ ), and wind speed ( $r = 0.15$ ,  $p < 0.01$ ). Important negative factors include  
390 VPD ( $r = -0.26$ ,  $p < 0.01$ ), SWC at all depths (varied  $r$  values between  $-0.17$  and  $-0.26$ ,  $p < 0.01$ ),  
391  $T_{air}$  ( $r = -0.11$ ,  $p < 0.01$ ), and air pressure ( $r = -0.15$ ,  $p < 0.01$ ). The correlation signal between  
392  $CH_4$  fluxes and  $T_{soil}$  changed with soil depths (varied  $r$  values between  $-0.09$  and  $0.24$ ,  $p <$   
393  $0.01$ ). Furthermore, path analysis results showed that  $T_{soil}$  at 5cm and 10cm were the most  
394 important factors, which together contributed about 25% of the relative importance coefficient.  
395 Following these factors in importance were SWC at 80 cm (14%) and 20 cm (12%), and  $T_{soil}$  at  
396 20 cm (8%).

397 Further analyses suggested that dominant control factors of CH<sub>4</sub> fluxes also changed  
398 among different seasons. In spring<sub>-</sub>, Rn was the most important factor, with a relative  
399 importance coefficient near 60%, followed by SHF at 5 cm (9%), and SWC at 20 cm (6%). Table  
400 4 shows the results of PCA. In spring<sub>-</sub>, PC1 explained 63% of the CH<sub>4</sub> variations, which was  
401 positively correlated with Tair, VPD, Rn, SHF of 15 cm, ALT, ΔI, SWC of 10 – 40 cm, Tsoil of  
402 0 cm, Tsoil of 5 – 20 cm, Tsoil of 30 – 50 cm, and negatively correlated with wind speed. The  
403 PC2 explained about 23% of CH<sub>4</sub> fluxes variations. PC2 was positively correlated with wind  
404 speed, Tair, Rn, SHF of 15cm, but negatively correlated with VPD, ALT, ΔI, SWC 10 – 40 cm,  
405 Tsoil of 0 cm, Tsoil of 5 – 20 cm, and Tsoil of 30 – 50 cm. The first four principal components  
406 explained about 86% of the CH<sub>4</sub> variations.

407 In summer<sub>-</sub>, CH<sub>4</sub> fluxes were most related with Tsoil at 100 cm and 200 cm, with an  
408 relative importance coefficient of about 30.2% and 26.5%, respectively. Other important  
409 environmental determinants of CH<sub>4</sub> fluxes were Tsoil at 70 cm (12.3%), and Tsoil at 0 – 20 cm  
410 (11.4%). The first four principal components explained about 88% of the CH<sub>4</sub> variations (Table  
411 4). PC1 explained 70% of the CH<sub>4</sub> variations. ~~PC1~~ was positively correlated with wind speed,  
412 Tair, VPD, SHF of 15 cm, ALT, ΔI, SWC of 50 – 160 cm, precipitation, Tsoil of 0 cm, Tsoil of 5  
413 – 40 cm, Tsoil of 50 – 80 cm, and Tsoil of 100 – 200 cm, but negatively correlated with Rn and  
414 SWC of 10 – 40 cm. PC2 was positively correlated with wind speed, Tair, VPD, Rn, SHF of  
415 15cm, SWC of 10 – 40 cm, Tsoil of 0 cm, but negatively correlated with ALT, ΔI, SWC of 50 –  
416 160 cm, precipitation, Tsoil of 5 – 40 cm, Tsoil of 50 – 80 cm, and Tsoil of 100 – 200 cm.

417 In autumn<sub>-</sub>, Rn and Tsoil at 5 – 20 cm had the highest relative importance coefficients  
418 for explaining the CH<sub>4</sub> flux variation. The first four principal components explained about 86%  
419 of the CH<sub>4</sub> variations (Table 4). PC1 explained 69% of the CH<sub>4</sub> variations. PC1 was positively

420 correlated with Tair, VPD, Rn, SHF of 15 cm, ALT, ΔI, SWC of 10 – 40 cm, SWC of 50 – 160  
421 cm, Tsoil of 0 cm, Tsoil of 5 – 40 cm, Tsoil of 50 – 80 cm, and Tsoil of 100 – 200 cm, but  
422 negatively correlated with wind speed. PC2 was positively correlated with wind speed, Tair, Rn,  
423 SHF of 15 cm, ALT, ΔI, Tsoil of 0 cm, and Tsoil of 5 – 40 cm, but negatively correlated with  
424 VPD, SWC of 10 – 40 cm, SWC of 50 – 60 cm, Tsoil of 50 – 80 cm, and Tsoil of 100 – 200 cm.

425 During winter, Rn was again the most important factor (34% relative importance  
426 coefficient), followed by Tsoil at 0 – 40 cm (27% in total), and SHF of 15 cm (17% in total), in  
427 determining CH<sub>4</sub> fluxes. The first four principal components explained about 96% of the CH<sub>4</sub>  
428 variations (Table 4). PC1 explained 75% of the CH<sub>4</sub> variations. PC1 was positively correlated  
429 with wind speed, Tair, VPD, Rn, SHF of 15 cm, ΔI, Tsoil of 0 cm, and Tsoil of 5 – 20 cm. PC2  
430 explained 21% of the CH<sub>4</sub> variations. PC2 was positively correlated with wind speed, Tair, Rn,  
431 SHF of 15 cm, and ΔI, but negatively correlated with VPD, Tsoil of 0 cm, and Tsoil of 5 – 20  
432 cm.

### 433 3.4 Empirical Model Comparison for Different CH<sub>4</sub> Flux Season Classification System

434 Lastly, we also compared how different season definitions, including the methods of  
435 SMT, VCT, JMC, and VPC, may have impacted the predictability of CH<sub>4</sub> fluxes. We established  
436 empirical maximum likelihood models between all environmental factors and diel CH<sub>4</sub> fluxes  
437 over each season, and then compared modeled CH<sub>4</sub> fluxes and field observations under those  
438 methods of different seasonal definitions (Figure 5). We found that the agreement between  
439 modeled and observed CH<sub>4</sub> fluxes, using the new SMT method, reached  $R^2 = 0.28$ , almost twice  
440 that of the VPC ( $R^2 = 0.17$ ) and VCT ( $R^2 = 0.14$ ) methods, and more than three times that of the  
441 JMC method ( $R^2 = 0.08$ ; Figure 5). Hence, the comparison suggested that our new method could  
442 better model CH<sub>4</sub> fluxes over a year. The use of the traditional plant growing season versus

443 nongrowing season definitions may also underestimate or overestimate CH<sub>4</sub> sinks or sources,  
444 especially when many studies assume CH<sub>4</sub> is close to zero during the plant nongrowing season.  
445 Furthermore, the new SMT method accurately captures the impact of spring<sub>m</sub> and autumn<sub>m</sub>  
446 permafrost thawing / freezing cycles on CH<sub>4</sub> fluxes, and the different preferable environments  
447 for methanogens and methanotrophic bacteria during the summer<sub>m</sub> season, while conventional  
448 methods do not.

## 449 **4. Discussion**

### 450 **4.1 Annual, Season mean and Diel Variability**

451 Our results suggested that the alpine steppe ecosystem in Beilu'he was a CH<sub>4</sub> sink of  
452 about  $-0.86 \pm 0.23 \text{ g CH}_4 - \text{C m}^{-2} \text{ yr}^{-1}$  during the study period of 2012-2016. This sink strength is  
453 larger than that of previous reports from other sites of the QTP (Cao et al., 2008; Wei et al.,  
454 2012; Li et al., 2012; Song et al., 2015; Chang and Shi, 2015), and many other high-latitude  
455 Arctic tundra ecosystems, like northeast Greenland (Jørgensen et al., 2015), western Siberia  
456 (Liebner et al., 2011), and Alaska (Whalen et al., 1992; Zhuang et al., 2004; Whalen, 2005).  
457 Different soil hydrothermal conditions, which previous studies have shown will greatly influence  
458 CH<sub>4</sub> cycles in permafrost regions (Spahni et al., 2011; Kirschke et al., 2013), may partly explain  
459 the site difference in CH<sub>4</sub> dynamics. For example, compared to the wet and often snow-covered  
460 high-latitude Arctic tundra ecosystems, there is no or little snow cover during the cold season in  
461 the QTP alpine steppes (Supplementary Table 1). During winter<sub>m</sub>, the Beilu'he meteorological  
462 data shows that the snow-cover time < 33.7h, SWC of 0-40cm within footprint < 7.6% from  
463 2012 to 2016 (Supplementary Table 1), is far below high-latitude Arctic tundra ecosystems.  
464 Jansson and Taş (2014) pointed out that relatively dry soils could facilitate the oxidation of CH<sub>4</sub>,  
465 since the increased number of gaps between soil particles in dry soils enhances the diffusion of

466 oxygen (O<sub>2</sub>) and CH<sub>4</sub> molecules and promotes aerobic respiration of soil microorganisms (Wang  
467 et al., 2014; Song et al., 2015). Meanwhile, unfrozen or capillary water found in cold-season  
468 permafrost soils ensures sufficient soil moisture for microbial activities, even in relatively drier  
469 and cold soils (Panikov and Dedysh, 2000; Rivkina et al., 2004). In addition, many previous  
470 studies used static chambers in CH<sub>4</sub> measurements, and may not have included a plant non-  
471 growing season (Wei et al., 2015a; Wang et al., 2014). Static chambers could underestimate CH<sub>4</sub>  
472 uptake because of the additional chamber heating-induced CH<sub>4</sub> emissions and frequent  
473 measurement gaps from overheating preventive shutdowns (Sturtevant et al., 2012).

474         We argued that seasonal freezing and thawing dynamics may be a key reason to explain  
475 the site's seasonal difference in CH<sub>4</sub> dynamics. Freezing and thawing processes are typical  
476 characteristics of the QTP permafrost (Wang et al., 2008; Wang et al., 2000; Qin et al., 2016).  
477 Our work suggests that freezing and thawing dynamics have played a critical role in governing  
478 permafrost seasonal and diel CH<sub>4</sub> cycling. For instance, while both spring- and autumn- are  
479 active seasons for the freeze-thaw dynamics of top soil layers and share many similarities, they  
480 have opposite CH<sub>4</sub> processes—soils emit CH<sub>4</sub> during spring- (Supplementary Figure 9-b), but  
481 consume CH<sub>4</sub> during autumn- (Supplementary Figure 9-d). We hypothesize that the difference  
482 in the freezing and thawing processes of the two seasons may have played a critical role in  
483 determining the direction of CH<sub>4</sub> dynamics. In spring-, the SWC of 10cm is 12.4%, 20-40cm is  
484 9.2%, 80cm is 11.4%, and 160cm is 13.6% (Supplementary Table 1), the active soil layer thaws  
485 from top to bottom (Jin et al., 2000; Cao et al., 2017), and the permafrost table is very shallow  
486 (about 10 ~ 45 cm), and is generally water proof (Wu and Zhang, 2008; Song et al., 2015; Lin  
487 et al., 2015). The water thawed during the day time would freeze again at night on the soil  
488 surface (Supplementary Figure 10-a; Shi et al., 2006; Wu and Zhang, 2010b). The thin-ice layer

489 could stop atmospheric gases of CH<sub>4</sub> and O<sub>2</sub> from getting into the soils (Gazovic et al., 2010).  
490 During autumn, the SWC of 10cm is 15.3%, 20-40cm is only 9.4%, but 80cm is 13.6%, and  
491 160cm can up to 21.0% (Supplementary Table 1), however, soils are bidirectionally frozen from  
492 both top (ground surface) and bottom, the permafrost table, which is about 200~400 cm deep ;  
493 (Supplementary Figure 8; Wu and Zhang, 2010a), doesn't form a layer of thin ice during the  
494 nighttime surface soil freezing, because on the one hand, the frozen soil of the ground surface  
495 (about 0-40cm) prevents the outside liquid water from permeating. On the other hand, the  
496 freezing itself will reduce the liquid water content in the soil (Ma et al., 2015). Therefore, it  
497 creates finely closed anaerobic gaps that allow CH<sub>4</sub> and O<sub>2</sub> gases into deep soils (about  
498 50~400cm; Mastepanov et al., 2008; Mastepanov et al., 2013; Zona et al., 2016). Meanwhile, the  
499 temperature of deep soils (about 50~400cm), still remains at a relatively high level  
500 (Supplementary Figure 10: b), and methanotrophic bacteria there are still active at this high Tsoil  
501 (Figure 2). This could be one important mechanism for autumn soil CH<sub>4</sub> consumption. In  
502 addition, in principal it was also possible that the observed seasonal variation in CH<sub>4</sub> flux may  
503 actually arise from the spatial variation of the footprint covered by the eddy covariance site  
504 (within 175m), given that prevalent wind direction changes seasonally (Supplementary Figure 4).  
505 Nonetheless, we found that the same vegetation species and soil exist in different directions to  
506 the tower within the footprint (Supplementary Figure 11). Hence this spatial vegetation and soil  
507 homogeneity further confirm that seasonal soil freezing and thawing differences may likely be  
508 the main explanation for seasonal CH<sub>4</sub> variations.

509 Furthermore, we suggested that the specific autumn soil vertical structure may help  
510 explain why the site was a CH<sub>4</sub> sink, unlike the CH<sub>4</sub> source in spring. The sequential probing  
511 data enables us to establish a rough estimate on the soil vertical structure during the autumn

512 thawing–freezing process, in which the vertical distribution of clay, sandy soils, and soil organic  
513 layers was mixed like a multi–layer hamburger structure, rather than forming a gradual change  
514 (Figure 6:e). As the soil profile has a different density, thermal conductivity, ~~heat of phase~~  
515 ~~transition~~, salinity of soil, ~~and so on~~, we boldly conjecture that, ~~similarly~~, the  $T_{\text{soil}}$ , SWC, and  
516 soil microbial activities also had this hamburger type of vertical distribution. As a result, layers  
517 of frozen and thawed soils were not changing gradually but appeared like a hamburger structure  
518 too. This ~~hamburger–like~~ soil vertical structure trapped high concentrations of soil water  
519 between the frozen layers, which was therefore highly anaerobic and suitable for  $\text{CH}_4$   
520 production. ~~Also, because of the hamburger–like structure, it fueled~~ speculation that biogenic  
521  $\text{CH}_4$  between frozen layers could not escape in autumn. The biogenic  $\text{CH}_4$  was trapped until the  
522 ACL soil layer was completely frozen in late autumn, and in some warmer years until early  
523 winter and created frost cracks. This enabled it to escape and may explain why there was a large  
524 burst of  $\text{CH}_4$  emissions in late autumn and early winter and may also explain the constant  
525 weak  $\text{CH}_4$  emission through the winter season, although methanogenic bacteria may have  
526 stopped functioning in the low temperature of winter. Of course, ~~this will need~~ further study  
527 and necessitates direct data collection in the field.

## 528 **4.2 Impacts of Environmental, Permafrost, and Microbial Activities on $\text{CH}_4$ Fluxes**

529 Our results demonstrated the important roles of climate, freezing and thawing dynamics,  
530 and soil microbe activities in regulating the direction and amount of  $\text{CH}_4$  exchanges between the  
531 atmosphere and ecosystems in permafrost areas. The key role of the above factors and processes  
532 was also confirmed by the better representation of seasonal  $\text{CH}_4$  cycles by our new seasonal  
533 division method based on soil microbes, temperature, and permafrost dynamics rather than  $T_{\text{air}}$   
534 or vegetation phenology. Here, we further discuss potential mechanisms of how environmental



535 (including air and soil heat and water), freezing and thawing processes, and soil microbes control  
536 the production and absorption of CH<sub>4</sub>.


537 First, it is noteworthy that both the strength and direction of correlations between CH<sub>4</sub>  
538 fluxes, SWC, and T<sub>soil</sub> parameters changed with soil depths, particularly during spring\_ and  
539 autumn\_, when active layer soils shifted between thawing and freezing regularly. The positive  
540 and negative CH<sub>4</sub> flux correlations with T<sub>soil</sub> and SWC may suggest that the impacts of T<sub>soil</sub>  
541 and SWC on CH<sub>4</sub> fluxes shall be treated as a holistic process, rather than as separate ones. For  
542 instance, in autumn\_, the correlation between CH<sub>4</sub> fluxes and T<sub>soil</sub> or SWC was positive at some  
543 soil depths, but negative at some other depths, reaching the maximum at the depth of 80 cm.  
544 Further, *in situ* observations suggested that soil organic matter and soil microbe amount were  
545 also at a very high level at this depth, highlighting that the regulation of soil abiotic factors on  
546 CH<sub>4</sub> cycling may be well influenced by soil biotic activities. In addition, the holistic soil heat–  
547 water process could also determine the concentration of soil inorganic ions, particularly during  
548 spring\_ and autumn\_, which were critical factors controlling the amount of soil unfrozen water.  
549 Soil unfrozen water in winter perhaps being important for maintaining soil microbial activities  
550 (Panikov and Dedysh, 2000; Rivkina et al., 2004); and in the future work we will include data  
551 acquiring of soil unfrozen water and test its role in regulating CH<sub>4</sub> exchanges in permafrost  
552 regions.

553 T<sub>air</sub> and precipitation impact CH<sub>4</sub> fluxes indirectly through their influences on T<sub>soil</sub> and  
554 SWC (Zhuang et al., 2004; Lecher et al., 2015). Such indirect influences may often be  
555 characterized with time–lagged effects (Koven et al., 2011). For instance, post–drought rainfall  
556 events in summer\_ can first promote soil CH<sub>4</sub> consumption (summer\_ of 2014). This is because  
557 certain soil moisture is needed for methanogenic bacteria to function (Del et al., 2000; Luo et al.,

558 2012). Yet, prolonged rainfall will eventually cause CH<sub>4</sub> fluxes to change from negative (soils  
559 consume CH<sub>4</sub>) to positive (soils emit CH<sub>4</sub>) fluxes (for example, 168<sup>th</sup> to 183<sup>th</sup> of 2015, Figure 3:  
560 d). After rainfall events, CH<sub>4</sub> flux gradually turned negative again with the decrease of SWC. As  
561 a result of these time-lagged effects, the correlation coefficient between CH<sub>4</sub> fluxes and  
562 precipitation often appears very low, although still statistically significant.

563         Second, soil methanogenic and methanotrophic bacteria could co-exist with different  
564 optimal niches (e.g., ranges of T<sub>air</sub> / T<sub>soil</sub> and SWC; Zhuang et al., 2013; Lau et al., 2015; Wei  
565 et al., 2015a). For example, the CH<sub>4</sub> diel cycle in summer<sub>=</sub> was found to have two strong  
566 consumption peaks and one weak emission peak (Figure 4: a3, c3, d3, e3). The timing of these  
567 different peaks may well reflect the different environmental requirements for the dominance of  
568 methanogens and methanotrophic bacteria. Furthermore, methanogens may have a broader  
569 functional temperature range than methanotrophic bacteria (Kolb, 2009; Lau et al., 2015; Yang et  
570 al., 2016). This is also evident, for example, from the diel CH<sub>4</sub> cycle in autumn<sub>=</sub> when CH<sub>4</sub>  
571 consumption was minimal at both lowest and highest T<sub>air</sub> (Figure 4: a4, b4, c4, d4, e4).

572         The complex relationships between CH<sub>4</sub> fluxes and environmental factors make it a grand  
573 challenge to predict the future of the QTP CH<sub>4</sub> budget under a changing climate. For instance, it  
574 has been generally believed that the ALT will increase under projected warming (Wu and Liu,  
575 2004). The positive correlation between CH<sub>4</sub> fluxes and ALT found here suggests that the QTP  
576 permafrost CH<sub>4</sub> sink may thus be weakened. However, the negative correlation between CH<sub>4</sub>  
577 flux and T<sub>air</sub> may lead to a different conclusion. Incorporating our findings and high-resolution  
578 data into mechanistic CH<sub>4</sub> models is therefore needed to enhance our capacity in predicting  
579 future CH<sub>4</sub> budgets. Earth system models have been introduced to estimate CH<sub>4</sub> dynamics  
580 (Curry, 2007; Spahni et al., 2011; Bohn et al., 2015). For example, using a terrestrial ecosystem

581 modelling approach, Zhuang et al. (2004) estimated the average QTP permafrost CH<sub>4</sub> sink of -  
582 0.08 g C m<sup>-2</sup> yr<sup>-1</sup>, much smaller than our field-based CH<sub>4</sub> estimate (-0.86 ± 0.23 g CH<sub>4</sub>-C m<sup>-2</sup> yr<sup>-1</sup>).  
583 Current CH<sub>4</sub> models focus on the regulation of CH<sub>4</sub> processes by temperature and SWC, and  
584 usually lack high-resolution data for model parameterization (Bohn et al., 2015). Data  
585 interpolation and the use of average values of certain environmental factors are normal practices  
586 in most models (Zhuang et al., 2004), which may overlook the impacts of environmental  
587 variations on CH<sub>4</sub> dynamics. For example, at Beilu'he, Tair on a typical summer day (e.g., July  
588 6<sup>th</sup>, 2013) could vary between -6 °C and 28 °C, a difference of 34 °C. The resulting diel mean  
589 temperature, 17 °C, is beyond the range of methanotrophic bacteria's preferable temperature of  
590 20~30 °C (Segers, 1998; Steinkamp et al., 2001; Yang et al., 2016). Therefore, models using  
591 diel mean temperature as an input may estimate the site as a net CH<sub>4</sub> sink. However, field  
592 observations show a source with a sink only during a short period (8:30am~11:30 am), on July  
593 6<sup>th</sup>, 2013, because the short period of the sink was offset by the source over the remaining 21  
594 hours. thermore, half-hourly SWC was well related with the waterproof role by the  
595 permafrost layer during spring and autumn (Figure 6-a). However, because of the shortage of  
596 high temporal resolution data, half-diel or diel mean SWC data are often used in many previous  
597 studies (Zhu et al., 2004; Jiang et al., 2010; Wei et al., 2015b), which could not correctly show  
598 the regulation of permafrost soil properties that are critical for CH<sub>4</sub> dynamics. As another  
599 example, Tsoil of 0 – 50 cm depth is one of the most important factors related to CH<sub>4</sub> fluxes  
600 (Mastepanov et al., 2008). However, many studies used Tair or re-analyzed deep Tsoil instead  
601 (Zhu et al., 2004; Bohn et al., 2015; Oh et al., 2016). Because the active layer is not  
602 homogeneous, but with different thermal conductivities during the freezing and thawing process,  
603 the use of Tair or deep Tsoil brings in large uncertainties in CH<sub>4</sub> modelling. Future research

604 needs to improve mechanistic understanding of CH<sub>4</sub> dynamics and their biotic and abiotic  
605 control factors, and to conduct more high-resolution and long-term field monitoring.

#### 606 **4.3 The Classification System of the Four Seasons for CH<sub>4</sub> Studies**

607 Our study ~~is also different~~ from the majority of earlier studies ~~in seasonal definitions~~  
608 (Treat et al., 2014; Wang et al., 2014; Wei et al., 2015a; Song et al., 2015). Here, we adopted a  
609 new classification system of the four seasons based on 0 – 25 cm soil depth bacterial activities  
610 (Figure 2), T<sub>soil</sub> of 0 – 40 cm (Supplementary Figure 6-a), and ALT (Supplementary Figure 8),  
611 rather than the conventional methods based on T<sub>air</sub> and vegetation dynamics (Chen et al., 2011;  
612 McGuire et al., 2012). Previous studies indicated that changes in CH<sub>4</sub> fluxes are regulated by soil  
613 microbes, and activities of soil microbes are not limited to the warm season (Zhuang et al., 2004;  
614 Lau et al., 2015; Yang et al., 2016). For instance, in March and November, we found the amount  
615 of gene expression by methanogens and methanotrophs at 0 – 25 cm soils were about 16.8% and  
616 35.6% (Figure 2), respectively, suggesting there are still strong microbial activities during the  
617 cold and dry season. Therefore, our new method of defining the four seasons from the top soil's  
618 biotic and abiotic features better captures the pattern of CH<sub>4</sub> dynamics throughout a year.

#### 619 **5. Conclusions**

620 Our field data indicates that there was a large CH<sub>4</sub> sink in the QTP permafrost area during  
621 recent years. The strength of this CH<sub>4</sub> sink is larger than previous studies in the region and many  
622 high-latitude tundra ecosystems. This study highlights the complexity of environmental controls,  
623 including soil heat-water processes, permafrost freezing and thawing dynamics, and soil  
624 microbial activities, on CH<sub>4</sub> cycling. This complexity implies that linear interpolation and  
625 extrapolation from site-level studies could introduce large uncertainties in CH<sub>4</sub> flux estimation.  
626 Future quantification of CH<sub>4</sub> dynamics in permafrost regions needs to account for the effects of

627 complex environmental processes, including freezing and thawing, and the interaction between  
628 heat and water, as well as microbial activities. Our findings also highlight the importance of  
629 conducting more high-resolution and long-term field monitoring in permafrost regions for better  
630 understanding and modelling of permafrost CH<sub>4</sub> cycling under a changing climate.

### 631 **Acknowledgements**

632 We would like to thank Yongzhi Liu, Jing Luo, Ji Chen, Guilong Wu, Wanan Zhu, Zhipeng  
633 Xiao, and Chang Liao for their tremendous help in collecting field data over all these years. We  
634 also want to pay tribute and gratitude to the late Xiaowen Cui for his contribution to our many  
635 field adventures. We thank John McCabe for proofreading the manuscript. This study was  
636 supported by the National Natural Science Foundation of China (41501083), Opening Research  
637 Foundation of Key Laboratory of Land Surface Process and Climate Change in Cold and Arid  
638 Regions, Chinese Academy of Sciences (LPCC201307), and Opening Research Foundation of  
639 Plateau Atmosphere and Environment Key Laboratory of Sichuan Province (PAEKL – 2014 –  
640 C3). A. C. acknowledges the support from a Purdue University Forestry and Natural Resources  
641 research scholarship. The data generated in this study will be freely available on the Asia Flux  
642 regional network server (<https://db.cger.nies.go.jp/asiafluxdb/>).

### 643 **Reference**

644 Bohn T., Melton J., Ito A.: WETCHIMP–WSL: intercomparison of wetland methane emissions  
645 models over West Siberia, *Biogeosciences*, 12, 3321 – 3349, 2015.

646 Burba, G. G., Mcdermitt, D. K., and Grelle, A.: Addressing the influence of instrument surface  
647 heat exchange on the measurements of CO<sub>2</sub> flux from open-path gas  
648 analyzers. *Glob. Change Biol.*, 14(8), 1854 – 1876, 2008.

649 Cao G., Xu X., and Long R.: Methane emissions by alpine plant communities in the Qinghai–  
650 Tibet Plateau, *Biol. Lett.*, 4, 681 – 684, 2008.

651 Cao B., Gruber S., Zhang T.: Spatial variability of active layer thickness detected by ground–  
652 penetrating radar in the Qilian Mountains, Western China, *J. Geophys. Res. Earth Surf.*,  
653 122, 574 – 591, 2017.

654 Cate, R. B., and Nelson, L. A.: A simple statistical procedure for partitioning soil test correlation  
655 data into two classes, *Soil Sci. Soc. Am. J.*, 35(4), 658 – 660, 1971.

656 Chang R., Miller C., and Dinardo S.: Methane emissions from Alaska in 2012 from CARVE  
657 airborne observations, *Proc. Natl. Acad. Sci. U. S. A.*, 111, 16694 – 16699, 2014.

658 Chang S. and Shi P.: A review of research on responses of leaf traits to climate change, *Chin. J.*  
659 *Plant Ecol.*, 39, 206 – 216, 2015.

660 Chen W., Wolf B., and Zheng X.: Annual methane uptake by temperate semiarid steppes as  
661 regulated by stocking rates, aboveground plant biomass and topsoil air permeability.  
662 *Glob. Change Biol.*, 17, 2803 – 2816, 2011.

663 Curry C.: Modeling the soil consumption at atmospheric methane at the global scale. *Glob.*  
664 *Biogeochem. Cycles*, 21, 1 – 15, 2007.

665 Dengel S., Zona D., and Sachs T.: Testing the applicability of neural networks as a gap–filling  
666 method using CH<sub>4</sub> flux data from high latitude wetlands. *Biogeosciences*, 10, 8185 – 8200,  
667 2013.

668 Del G., Parton W., and Mosier A.R.: General CH<sub>4</sub> oxidation model and comparisons of CH<sub>4</sub>  
669 oxidation in natural and managed systems, *Glob. Biogeochem. Cycles*, 14, 999 – 1019,

670 2000.

671 Falge, E., Baldocchi, D., and Olson, R.: Gap filling strategies for defensible annual sums of net  
672 ecosystem exchange, *Agric. For. Meteorol.*, 107(1), 43 – 69, 2001.

673 Gažovič M., Kutzbach L., and Schreiber P.: Diurnal dynamics of CH<sub>4</sub> from a boreal peatland  
674 during snowmelt. *Tellus, B*, 62, 133 – 139, 2010.

675 IPCC, climate change 2013: the physical science basis. Contribution of working group I to the  
676 fifth assessment report of the intergovernmental panel on climate change., 2013.

677 Jansson, J. K. and Tas, N.: The microbial ecology of permafrost, *Nat. Rev. Microbiol.*, 12, 414,  
678 2014.

679 Jiang C., Yu G., and Fang H.: Short-term effect of increasing nitrogen deposition on CO<sub>2</sub>, CH<sub>4</sub>  
680 and N<sub>2</sub>O fluxes in an alpine meadow on the Qinghai–Tibetan Plateau, China, *Atmos.*  
681 *Environ.*, 44, 2920 – 2926, 2010.

682 Jin H., Li S., and Cheng G.: Permafrost and climatic change in China, *Glob. Planet, Change*, 26,  
683 387 – 404, 2000.

684 Jørgensen, C. J., Johansen, K. M. L., and Westergaard–Nielsen, A.: Net regional methane sink in  
685 High Arctic soils of northeast Greenland, *Nat. Geosci.*, 8, 20, 2015.

686 Kirschke, S., Bousquet, P., and Ciais, P.: Three decades of global methane sources and  
687 sinks, *Nat. Geosci.*, 6, 813, 2013.

688 Kolb, S.: The quest for atmospheric methane oxidizers in forest soils, *Environ. Microbiol.*  
689 *Rep.*, 1, 336 – 346, 2009

690 Koven C.D., Ringer B., and Friedlingstein P.: Permafrost carbon–climate feedbacks accelerate

691 global warming, *Proc. Natl. Acad. Sci. U. S. A.*, 108, 14769 – 14774, 2011.

692 Lau M., Stackhouse B.T., and Layton A.C.: An active atmospheric methane sink in high Arctic  
693 mineral cryosols. *ISME J.*, 9, 1880 – 1891, 2015.

694 Lecher A.L., Dimova N., and Sparrow K.J.: Methane transport from the active layer to lakes in  
695 the Arctic using Toolik Lake, Alaska, as a case study, *Proc. Natl. Acad. Sci. U. S. A.*, 112,  
696 3636 – 3640, 2015.

697 Lee, X., Massman, W., and Law, B. (Eds.): *Handbook of micrometeorology: a guide for surface*  
698 *flux measurement and analysis (Vol. 29)*, Springer Science and Business Media, 2006.

699 Li K., Gong Y., and Song W.: Responses of CH<sub>4</sub>, CO<sub>2</sub> and N<sub>2</sub>O fluxes to increasing nitrogen  
700 deposition in alpine grassland of the Tianshan Mountains, *Chemosphere*, 88, 140 – 143,  
701 2012.

702 Liebner S., Zeyer J., and Wagner D.: Methane oxidation associated with submerged brown  
703 mosses reduces methane emissions from Siberian polygonal tundra, *J. Ecol.*, 99, 914 – 922,  
704 2011.

705 Lin Z., Burn C.R., and Niu F.: The Thermal Regime, including a Reversed Thermal Offset, of  
706 Arid Permafrost Sites with Variations in Vegetation Cover Density, Wudaoliang Basin,  
707 Qinghai–Tibet Plateau. *Permafr. Periglac. Process.*, 26, 142 – 159, 2015.

708 Loescher, H. W., Law, B. E., and Mahrt, L: Uncertainties in, and interpretation of, carbon flux  
709 estimates using the eddy covariance technique. *J. Geophys. Res. Atmos.*, 111(D21), 2006.

710 Luo G.J., Brüggemann N., and Wolf B.: Decadal variability of soil CO<sub>2</sub>, NO, N<sub>2</sub>O, and CH<sub>4</sub>  
711 fluxes at the Höglwald Forest, Germany. *Biogeosciences*, 9, 1741 – 1763, 2012.



712 Mastepanov M., Sigsgaard C., and Dlugokencky E.J.: Large tundra methane burst during onset  
713 of freezing. *Nature*, 456, 628 – 30, 2008.

714 Mastepanov, M., Sigsgaard, C., and Tagesson, T.: Revisiting factors controlling methane  
715 emissions from high-Arctic tundra, *Biogeosciences*, 10(7), 5139, 2013.

716 Ma W., Zhang L., and Yang C.: Discussion of the applicability of the generalized Clausius–  
717 Clapeyron equation and the frozen fringe process, *Earth-Sci. Rev.*, 142, 47-59, 2015.

718 Mauder, M., Cuntz, M., and Drüe, C.: A strategy for quality and uncertainty assessment of long–  
719 term eddy–covariance measurements. *Agric. For. Meteorol.*, 169, 122 – 135, 2013.

720 McGuire A.D., Christensen T.R., and Hayes D.: An assessment of the carbon balance of Arctic  
721 tundra: Comparisons among observations, process models, and atmospheric inversions,  
722 *Biogeosciences*, 9, 3185 – 3204, 2012.

723 Moncrieff, J., Clement, R., and Finnigan, J.: Averaging, detrending, and filtering of eddy  
724 covariance time series. In *Handbook of micrometeorology* (pp. 7 – 31), Springer  
725 Netherlands, 2004.

726 Muller, S. W. *Permafrost or permanently frozen ground and related engineering problems*, 1947.

727 Oh Y., Stackhouse B., and Lau M.: A scalable model for methane consumption in arctic mineral  
728 soils. *Geophys. Res. Lett.*, 43, 5143 – 5150, 2016.

729 Panikov N.S. and Dedysh S.N.: Cold season CH<sub>4</sub> and CO<sub>2</sub> emission from boreal peat bogs (West  
730 Siberia): Winter fluxes and thaw activation dynamics, *Glob. Biogeochem. Cycles*, 14, 1071  
731 – 1080, 2000.

732 Papale, D., Reichstein, M., and Aubinet, M.: Towards a standardized processing of Net

733 Ecosystem Exchange measured with eddy covariance technique: algorithms and uncertainty  
734 estimation. *Biogeosciences*, 3(4), 571 – 583, 2006.

735 Patra P.K. and Kort E.A.: Regional Methane Emission Estimation Based on Observed  
736 Atmospheric Concentrations (2002 – 2012), *J. Meteor. Soc. Japan. Ser. II*, 94, 91 – 113,  
737 2016.

738 Qin, Y., Wu T., and Li R., Using ERA-Interim reanalysis dataset to assess the changes of ground  
739 surface freezing and thawing condition on the Qinghai–Tibet Plateau. *Environ. Earth Sci.*,  
740 75(9): 1-13, 2016.

741 Rigby M., Prinn R.G., and Fraser P.J.: Renewed growth of atmospheric methane, *Geophys. Res.*  
742 *Lett.*, 35, 2 – 7, 2008.

743 Rivkina E., Laurinavichius K., and McGrath J.: Microbial life in permafrost, *Adv. Space Res.*,  
744 33, 1215 – 1221, 2004.

745 Segers R.: Methane production and methane consumption—a review of processes underlying  
746 wetland methane fluxes [Review], *Biogeochem.*, 41, 23 – 51, 1998.

747 Shi P., Sun X., and Xu L.: Net ecosystem CO<sub>2</sub> exchange and controlling factors in a steppe–  
748 Kobresia meadow on the Tibetan Plateau. *Sci. China Ser. D-Earth Sci.*, 49, 207 – 218, 2006.

749 Song, W., Wang, H., and Wang, G.: Methane emissions from an alpine wetland on the Tibetan  
750 Plateau: Neglected but vital contribution of the non–growing season, *J. Geophys. Res.*  
751 *Biogeosci.*, 120, 1475 – 1490, 2015.

752 Spahni R., Wania R., and Neef L.: Constraining global methane emissions and uptake by  
753 ecosystems. *Biogeosciences*, 8, 1643 – 1665, 2011.

754 Steinkamp R., Butterbach–Bahl K., and Papen H.: Methane oxidation by soils of an N limited  
755 and N fertilized spruce forest in the Black Forest, Germany, *Soil. Biol. Biochem.*, 33, 145 –  
756 153, 2001.

757 Sturtevant C.S., Oechel W.C., and Zona D.: Soil moisture control over autumn season methane  
758 flux, Arctic Coastal Plain of Alaska, *Biogeosciences*, 9, 1423 – 1440, 2012.

759 Treat C.C., Wollheim W.M., and Varner R.K.: Temperature and peat type control CO<sub>2</sub> and CH<sub>4</sub>  
760 production in Alaskan permafrost peats, *Glob. Chang. Biol.* 20, 2674 – 2686, 2014.

761 Vickers, D., and Mahrt, L.: Quality control and flux sampling problems for tower and aircraft  
762 data. *J. Atmos. Ocean. Technol.*, 14(3), 512 – 526, 1997.

763 Wang G., Li Y., and Wang Y.: Effects of permafrost thawing on vegetation and soil carbon pool  
764 losses on the Qinghai–Tibet Plateau, China, *Geoderma*, 143, 143 – 152, 2008.

765 Wang S., Jin H., Li S.: Permafrost degradation on the Qinghai–Tibet Plateau and its  
766 environmental impacts. *Permafr. Periglac. Process.*, 11, 43 – 53, 2000.

767 Wang Y., Liu H., and Chung H.: Non–growing season soil respiration is controlled by freezing  
768 and thawing processes in the summer monsoon-dominated Tibetan alpine grassland. *Glob.*  
769 *Biogeochem. Cycles*, 28, 1081 – 1095, 2014.

770 Wei D., Ri X., and Wang Y.: Responses of CO<sub>2</sub>, CH<sub>4</sub> and N<sub>2</sub>O fluxes to livestock enclosure in an  
771 alpine steppe on the Tibetan Plateau, China. *Plant Soil*, 359, 45 – 55, 2012.

772 Wei D., Ri X., and Tarchen T.: Considerable methane uptake by alpine grasslands despite the  
773 cold climate: In situ measurements on the central Tibetan Plateau, 2008 – 2013, *Glob.*  
774 *Chang Biol.*, 21, 777 – 788, 2015a.

775 Wei D., Tarchen T., and Dai D.: Revisiting the role of CH<sub>4</sub> emissions from alpine wetlands on  
776 the Tibetan Plateau: Evidence from two in situ measurements at 4758 and 4320 m above sea  
777 level, *J. Geophys. Res. Biogeosci.*, 120, 1741 – 1750, 2015b.

778 Whalen, S. C. and Reeburgh, W. S.: Consumption of atmospheric methane by tundra  
779 soils. *Nature*, 346, 160, 1990.

780 Whalen S.C.: Biogeochemistry of Methane Exchange between Natural Wetlands and the  
781 Atmosphere. *Environ. Eng. Sci.*, 22, 73 – 94, 2005.

782 Whalen S.C., Reeburgh W.S., and Barber V.A.: Oxidation of methane in boreal forest soils: a  
783 comparison of seven measures. *Biogeochemistry*, 16, 181 – 211, 1992.

784 Wu Q. and Liu Y.: Ground temperature monitoring and its recent change in Qinghai–Tibet  
785 Plateau, *Cold Reg. Sci. Technol.*, 38, 85 – 92, 2004.

786 Wu Q. and Zhang T.: Recent permafrost warming on the Qinghai–Tibetan Plateau. *J. Geophys.*  
787 *Res. Atmos.* 113, 1 – 22, 2008.

788 Wu Q. and Zhang T.: Changes in active layer thickness over the Qinghai–Tibetan Plateau from  
789 1995 to 2007, *J. Geophys. Res. Atmos.*, 115, D09107, 2010a.

790 Wu Q. Zhang T., and Liu Y.: Permafrost temperatures and thickness on the Qinghai–Tibet  
791 Plateau, *Glob. Planet. Change*, 72, 32 – 38, 2010b.

792 Yang S., Wen X., and Shi Y.: Hydrocarbon degraders establish at the costs of microbial richness,  
793 abundance and keystone taxa after crude oil contamination in permafrost environments. *Sci.*  
794 *Rep.*, 6, 37473, 2016.

795 Zhu X., Zhuang Q., and Chen M.: Net exchanges of methane and carbon dioxide on the

796 Qinghai–Tibetan Plateau from 1979 to 2100. *Environ. Res. Lett.*, 10, 85007. 2004.

797 Zhuang Q., Melillo J.M., and Kicklighter D.W.: Methane fluxes between terrestrial ecosystems  
798 and the atmosphere at northern high latitudes during the past century: A retrospective  
799 analysis with a process–based biogeochemistry model. *Glob. Biogeochem. Cycles*, 18(3),  
800 2004.

801 Zhuang Q., Chen M., and Xu K.: Response of global soil consumption of atmospheric methane  
802 to changes in atmospheric climate and nitrogen deposition. *Glob. Biogeochem. Cycles*, 27,  
803 650 – 663, 2013.

804 Zona D., Gioli B., and Commane R.: Cold season emissions dominate the Arctic tundra methane  
805 budget. *Proc. Natl. Acad. Sci. U. S. A.*, 113, 40 – 45, 2016.

806

807

808

809

810

811

812

813

814

815

816 **Table 1.** Soil characteristics at the eddy covariance flux study site

Soil depth cm	Soil type	Gravel content g kg <sup>-1</sup>	SOC g kg <sup>-1</sup>	Microbial Numbers ×10 <sup>4</sup>	pH	DBD g cm <sup>-3</sup>	SWC %	Total N ×10 <sup>3</sup> mg kg <sup>-1</sup>
0 – 20	clay	22.3	2.8	3.44	8.7	1.75	18.26	0.87
20 – 50	Silty clay	12.6	1.7	3.82	8.4	1.73	11.52	1.02
50 – 120	silt and fine sand	3.4	1.3	3.67	8.4	1.72	12.57	1.18
120 – 160	silt and fine sand	2.8	26.4	5.44	5.1	1.68	24.69	2.46
160 – 200	silt and fine sand	1.6	13.6	4.39	6.8	1.68	22.45	2.03

817 **Note:** Gravel content diameter ≥ 0.5cm. SOC is soil organic content, DBD is dry bulk density, and

818 SWC is soil water content.

819

820

821

822

823

824

825

826

827

**Table 2.** Measurements of four seasons from 2012 to 2016

	Spring=	Summer=	Autumn=	Winter=	Plant growing season	Plant non-growing season
	Period; Total days	Period; Total days	Period; Total days	Period; Total days	Period; Total days	Period; Total days
	Days	Days	Days	Days	Days	Days
2012	50 – 142; 93	143 – 229; 87	230 – 323; 94	1 – 49, 324 – 366; 92	139 – 286; 148 <sup>a</sup> 122 – 305; 184 <sup>b</sup> 143 – 290; 148 <sup>c</sup>	1 – 138, 287 – 366; 218 <sup>a</sup> 1 – 121, 306 – 366; 182 <sup>b</sup> 1 – 142, 291 – 366; 218 <sup>c</sup>
2013	36 – 137; 102	138 – 224; 87	225 – 334; 110	1 – 35, 335 – 365; 66	139 – 287; 149 <sup>a</sup> 121 – 304; 184 <sup>b</sup> 127 – 297; 171 <sup>c</sup>	1 – 138, 288 – 365; 216 <sup>a</sup> 1 – 120, 305 – 365; 181 <sup>b</sup> 1 – 126, 298 – 365; 194 <sup>c</sup>
2014	49 – 127; 79	128 – 228; 101	229 – 309; 81	1 – 48, 310 – 365; 104	137 – 288; 152 <sup>a</sup> 121 – 304; 184 <sup>b</sup> 142 – 294; 153 <sup>c</sup>	1 – 136, 289 – 365; 213 <sup>a</sup> 1 – 120, 305 – 365; 181 <sup>b</sup> 1 – 141, 295 – 365; 212 <sup>c</sup>
2015	36 – 150; 115	151 – 224; 74	225 – 312; 88	1 – 35, 313 – 365; 88	145 – 288; 144 <sup>a</sup> 121 – 304; 184 <sup>b</sup> 136 – 295; 160 <sup>c</sup>	1 – 144, 289 – 365; 221 <sup>a</sup> 1 – 120, 305 – 365; 181 <sup>b</sup> 1 – 135, 296 – 365; 205 <sup>c</sup>
2016	47 – 161; 115	162 – 225; 64	226 – 299; 74	1 – 46, 300 – 366; 113	141 – 287; 147 <sup>a</sup> 122 – 305; 183 <sup>b</sup> 140 – 296; 157 <sup>c</sup>	1 – 140, 288 – 366; 219 <sup>a</sup> 1 – 120, 305 – 366; 182 <sup>b</sup> 1 – 139, 297 – 366; 209 <sup>c</sup>

829 **Note:** <sup>a</sup>, based on vegetation cover and temperature change (VCT) (Lund et al., 2010; Tang and Arnone, 2013; Song et al., 2015); <sup>b</sup>, based on Julian  
830 months (JMC) (Da et al., 2015); <sup>c</sup>, based on vegetation phenology change (VPC). Spring<sub>-</sub>, Summer<sub>-</sub>, Autumn<sub>-</sub>, Winter<sub>-</sub> are based on parameters of  
831 microbial activities, ALT variety coefficient and Tsoil (SMT).

832

833

834

835

836

837

838

839

840

841

842

843



**Table 3.** Correlation coefficients between CH<sub>4</sub> fluxes and environment factors on half-hour scales

Environment Factors	CH <sub>4</sub> Flux									
	Spring_		Summer_		Fall_		Winter_		2012 – 2016	
	r	n	r	n	r	n	r	n	r	n
T <sub>air</sub>	0.25**	24144	0.14**	19818	-0.16**	20959	0.32**	22224	-0.11**	87145
Wind Speed	0.31**	24144	-0.04**	19817	-0.20**	20959	0.32**	22224	0.15**	87144
VPD	-0.33**	18624	-0.21**	19263	-0.09**	16737	-0.21	18000	0.26**	69624
Rn	0.55**	24143	0.09**	19807	-0.33**	20913	0.51**	22224	0.09**	87087
Albedo	0.07**	24144	-0.01	19814	-0.08**	20913	0.10**	22224	0.02**	87095
SHF of 5cm	0.46**	24144	-0.08**	19818	-0.23**	20913	0.43**	22224	0.09**	87099
SHF of 15cm	0.36**	24144	-0.15**	19815	-0.23**	20913	0.33**	22224	0.08**	87096
SWC of 10cm	-0.16**	24144	-0.14**	19818	-0.06**	20959	0.00	22224	-0.25**	87145
SWC of 20cm	-0.15**	24144	-0.13**	19816	-0.07**	20959	0.11**	22224	-0.24**	87143
SWC of 40cm	-0.11**	24144	-0.02**	19818	0.07**	20959	0.06**	22224	-0.17**	87145
SWC of 80cm			-0.13**	19818	0.06**	20959				
SWC of 160cm			0.04**	19818	-0.11**	20959				
Precipitation			-0.02	16748	0.01 <sup>b</sup>	17888				
ALT	0.73**	23004	0.23**	19823	0.73**	21454			0.43**	64281

$\Delta I$	0.77**	100	0.57**	83	0.46**	89	0.23	93	0.49**	365
$\Delta II$	0.31**	100	0.66**	83	0.78**	89	0.19	93	0.52**	365
T <sub>soil</sub> of 0 cm	-0.06*	23004	0.13**	19823	0.07**	20366	0.13**	21711	0.11**	84904
T <sub>soil</sub> of 5 cm	0.15**	24144	0.15**	19808	-0.13**	21454	0.27**	22224	0.24**	87630
T <sub>soil</sub> of 10 cm	-0.03**	24144	0.12**	19808	0.08**	21454	0.16**	22224	0.13**	87630
T <sub>soil</sub> of 20 cm	-0.14**	24144	0.08**	19808	0.02**	21454	0.06**	22224	-0.09**	87630
T <sub>soil</sub> of 30 cm	-0.13**	23004	0.06**	19823	-0.02**	20366	0.07**	21711	-0.08**	84904
T <sub>soil</sub> of 40 cm	0.14**	24144	0.05**	19808	-0.01 <sup>b</sup>	21454	0.06**	22224	0.11**	87630
T <sub>soil</sub> of 50 cm			0.04**	19823	-0.05**	20366				
T <sub>soil</sub> of 70 cm			0.07**	19823	-0.05**	20366				
T <sub>soil</sub> of 80 cm			0.05**	19808	0.04**	21454				
T <sub>soil</sub> of 100 cm			0.10**	19823	-0.05**	21454				
T <sub>soil</sub> of 150 cm			0.09**	19823	-0.04**	20366				
T <sub>soil</sub> of 160 cm			0.10**	19808	0.01**	21454				
T <sub>soil</sub> of 200 cm			0.02**	19823	-0.02**	20366				

845 **Note:** \*\* means  $p < 0.01$ , \* means  $p < 0.05$ ; r values for the relationship between CH<sub>4</sub> flux and environment factors. Tair means air temperature of 3 m  
846 above the ground surface. VPD is vapor pressure deficit, NR is net radiation, and SWC is soil water content, ALT is active layer thickness, which fitted  
847 through the depth of soil 0 °C in Surfer 8.0., and the data is removed as meaningless in winter. Tsoil is the temperature of the soil. In spring\_ and

848 winter\_, precipitation data is too sparse for statistical analysis.  $\Delta I$  is the soil 0 – 25cm archaeal methanogens gene expression, and  $\Delta II$  is the soil 0 – 25  
849 cm methanotrophic gene expression. The coefficients (r) between  $CH_4$  flux and  $\Delta I$ ,  $\Delta II$  are obtained using the synchronous  $CH_4$  fluxes averaged for 5  
850 days.

851

852

853

854

855

856

857

858

859

860

861

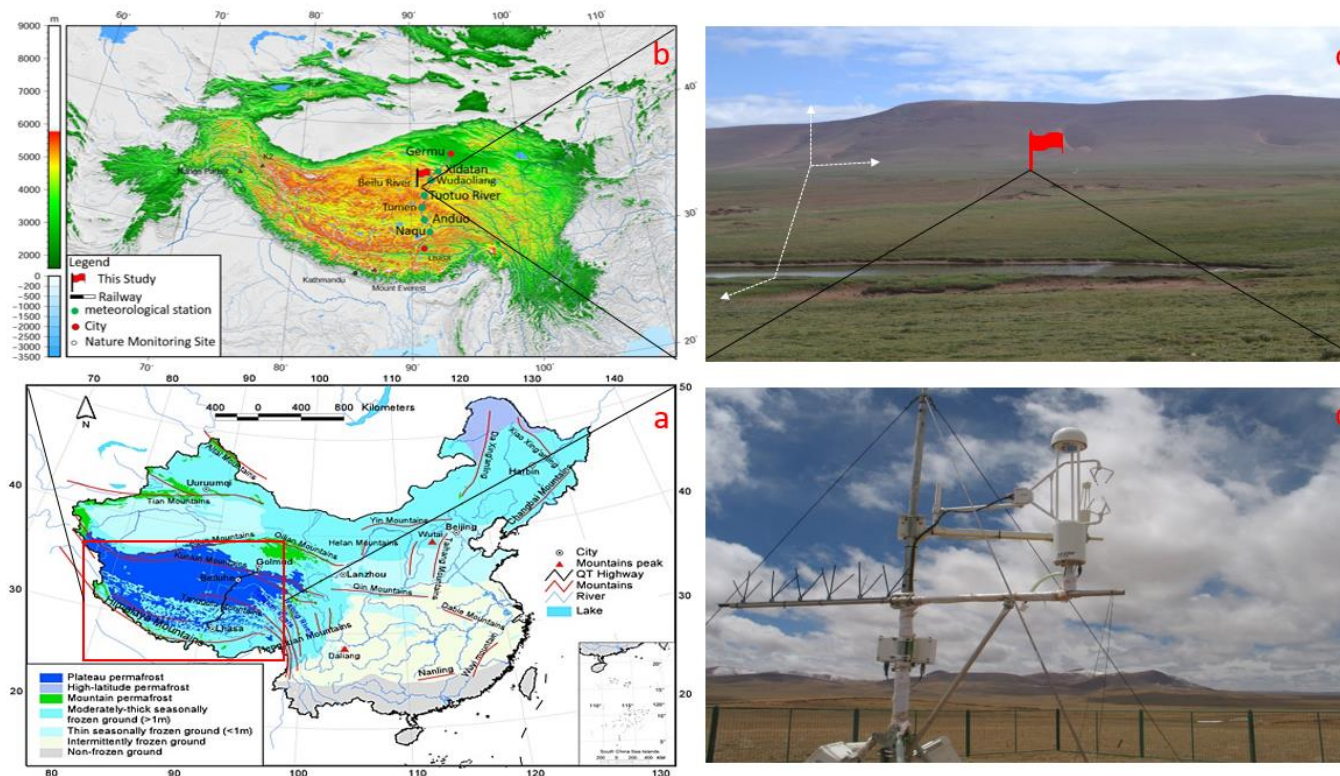
**Table 4.** Principal components analysis (PCA) of the environmental factors.

Component	Spring_				Summer_				autumn_				Winter_			
	PC1	PC2	PC3	PC4	PC1	PC2	PC3	PC4	PC1	PC2	PC3	PC4	PC1	PC2	PC3	PC4
wind speed	-0.03	0.51	0.65	-0.46	0.02	0.37	0.38	-0.13	-0.04	0.44	0.59	0.67	0.27	0.45	-0.11	-0.27
Tair	0.38	0.29	-0.05	-0.11	0.42	0.22	-0.03	0.02	0.36	0.21	0.08	-0.06	0.48	0.12	-0.02	0.01
VPD	0.34	-0.27	0.40	0.15	0.17	0.46	-0.22	0.09	0.34	-0.15	0.17	-0.07	0.14	-0.15	0.95	-0.22
Rn	0.16	0.49	0.00	0.76	-0.01	0.07	0.58	0.11	0.12	0.54	-0.43	-0.07	0.26	0.47	-0.01	-0.49
SHF of 15cm	0.24	0.49	-0.30	-0.09	0.25	0.53	-0.09	0.01	0.15	0.59	-0.23	-0.15	0.36	0.37	0.14	0.58
ALT	0.22	-0.40	0.40	0.27	0.32	-0.53	-0.05	0.02	0.29	0.49	0.70	0.25				
$\Delta I$	0.49	-0.22	0.01	-0.08	0.50	-0.16	0.02	-0.16	0.29	0.31	0.24	-0.51	0.52	0.05	0.07	-0.03
SWC of 10 – 20cm													-0.31	0.45	0.22	0.47
SWC of 10 – 40cm	0.33	-0.20	0.50	0.25	-0.16	0.15	-0.16	0.73	0.28	-0.18	-0.41	0.53				
SWC of 50 – 160cm					0.23	-0.20	-0.16	0.55	0.31	-0.17	-0.32	0.41				
Precipitation					0.03	-0.04	0.63	0.35								
Tsoil of 0 cm	0.43	-0.07	-0.20	-0.27	0.43	0.08	0.08	-0.07	0.37	0.07	0.19	-0.16	0.43	-0.35	-0.15	0.09
Tsoil of 5 – 20 cm	0.44	-0.01	-0.17	-0.16									0.45	-0.28	0.00	0.28
Tsoil of 5 – 40 cm					0.46	-0.05	0.04	-0.03	0.38	0.02	0.18	-0.17				
Tsoil of 30 – 50cm	0.40	-0.23	-0.08	-0.04												
Tsoil of 50 – 80cm					0.37	-0.36	0.00	0.01	0.37	-0.11	0.19	-0.14				
Tsoil of 100 – 200cm					0.33	-0.34	0.01	-0.01	0.36	-0.14	0.08	0.00				
Percent of variance	0.63	0.23	0.08	0.04	0.70	0.18	0.07	0.02	0.69	0.17	0.08	0.04	0.75	0.21	0.02	0.01
Cumulative	0.63	0.86	0.94	0.98	0.70	0.88	0.95	0.97	0.69	0.86	0.94	0.98	0.75	0.96	0.98	0.99

**Note:** PC means principal component. Before PCA, SWC was divided for three parts, 10 – 20 cm, 10 – 40 cm, and 50 – 160 cm according to collinearity

test in four seasons. Tsoil was divided for six parts of Tsoil of 0 cm, Tsoil of 5 – 20 cm, Tsoil of 5 – 40 cm, Tsoil of 30 – 50 cm, Tsoil of 50 – 80 cm,

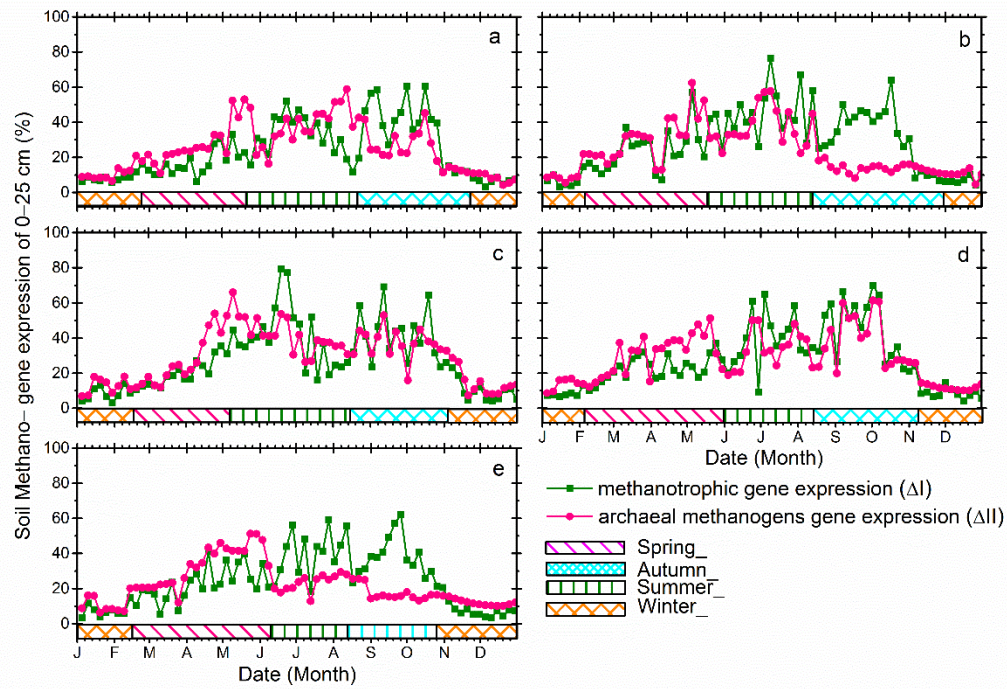
and Tsoil of 60 – 200 cm according to collinearity test in different seasons.



867

868 **Figure 1.** Geographic location of the study site: (a) is a map of China's permafrost distribution, and the red box marks the approximate location of  
 869 the Qinghai–Tibet Plateau; (b) shows the study site location and meteorological stations along the Qinghai–Tibet railway; (c) is the photo showing  
 870 the study site's topography and physiognomic. The small red flag in (c) is the eddy covariance tower location; (d) is the close-up shot of the LI-7700  
 871 for methane measurement. *Map boundary and location are approximate. Geographic features and the names do not imply any official endorsement*  
 872 *or recognition*

873



874

875

**Figure 2.** Annual patterns of soil methanogen-gene expression of 0 – 25 cm soil depth for years: (a) 2012, (b) 2013, (c) 2014, (d) 2015, and (e)

876

2016.

877

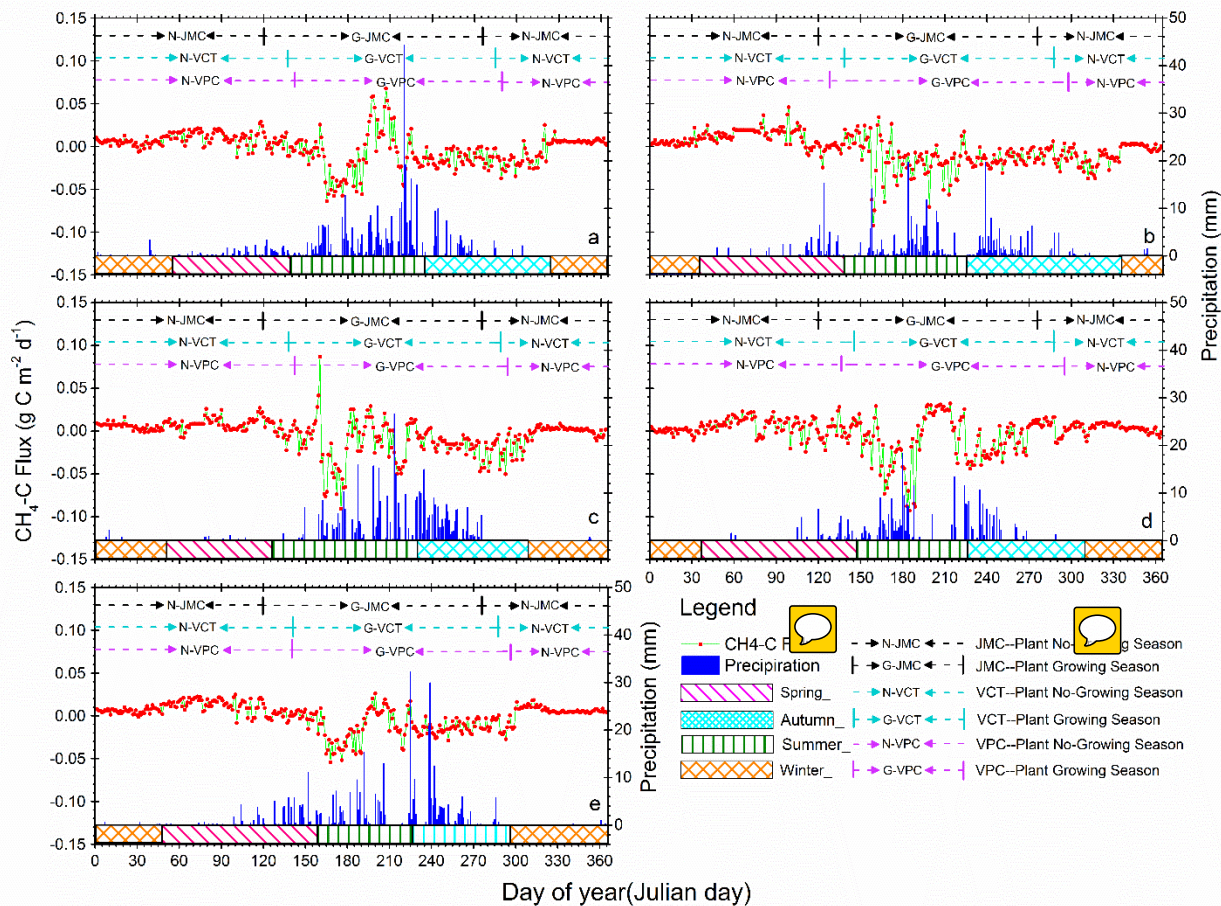
878

879

880

881

882

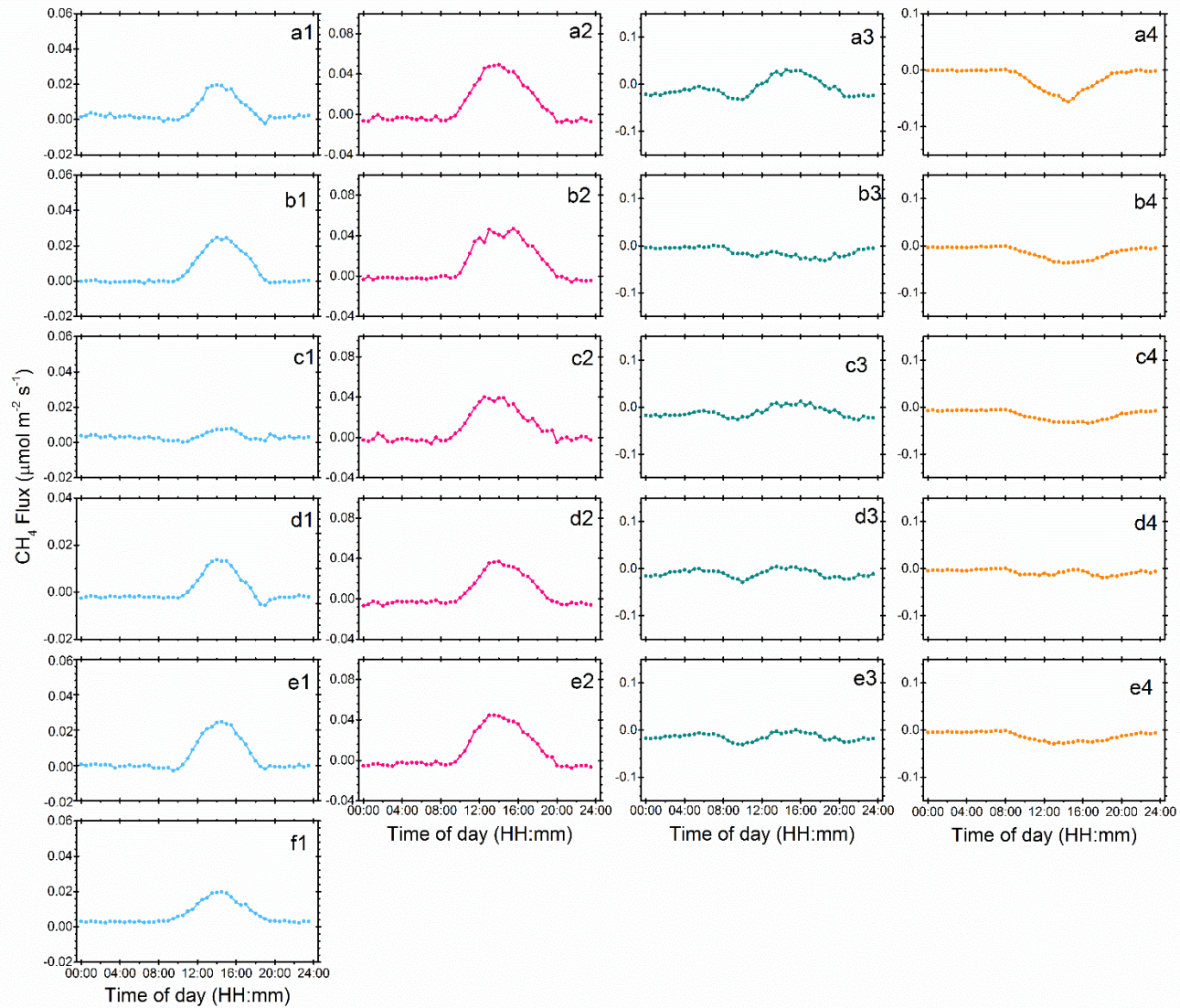


883

884 **Figure 3.** Annual patterns of diel methane ( $\text{CH}_4$ ) flux and precipitation variations from 2012 to 2016. Positive values indicate  $\text{CH}_4$  release and  
 885 negative values indicate  $\text{CH}_4$  uptake by ecosystems. Red dots and light green lines are  $\text{CH}_4\text{-C}$  flux variation, and the deep blue histograms show diel  
 886 precipitation accumulation. Pink, olive, cyan, and orange blocks mean spring, summer, autumn, and winter seasons respectively, according to our  
 887 new method of SMT (see Methods), . Black, cyan, and pink dotted lines with bars separated the plant growing from non-growing seasons and stand  
 888 for seasons by the method JMC, VCT, and VPC, respectively. Details about the methods JMC, VCT, and VPC can be found in [Text part 3.2](#).

889

890



891

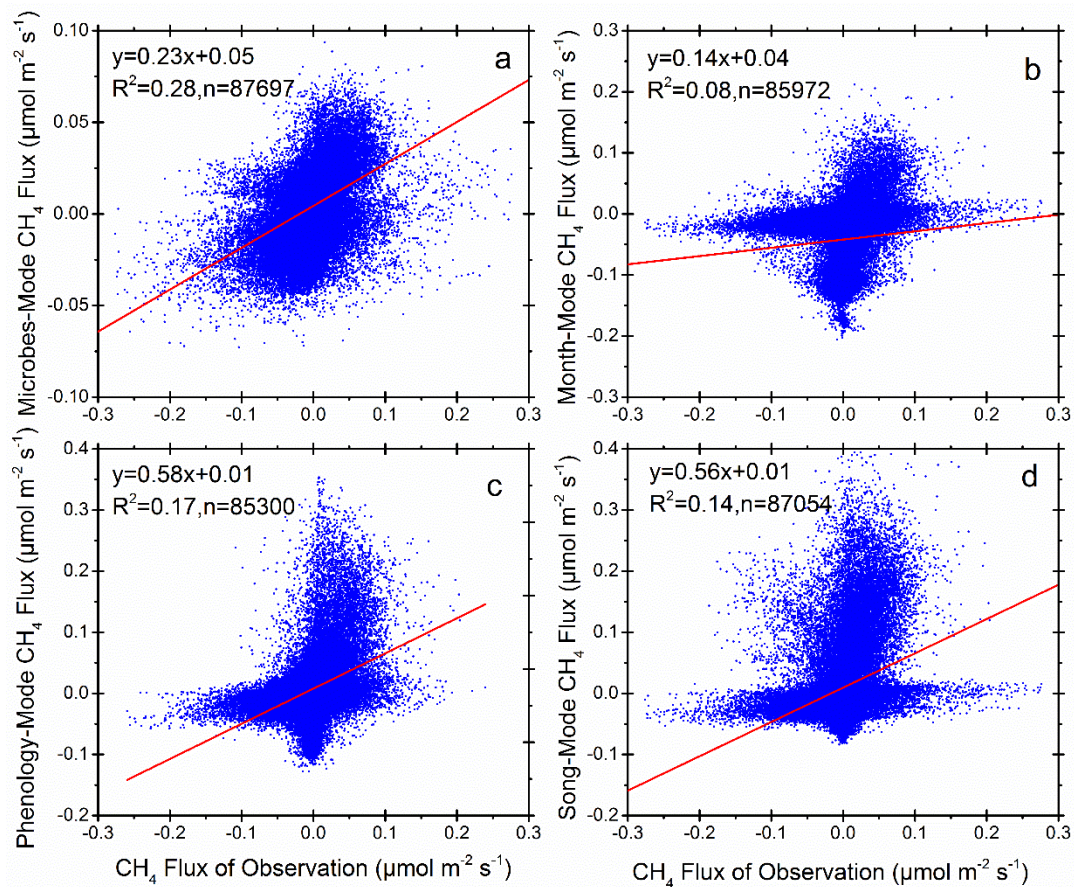
892

893

894

**Figure 4.** Diel CH<sub>4</sub> fluxes from 2012 to 2016 for different seasons. Blue, pink, green and orange, represent winter, spring, summer, and autumn, respectively; (a1), (a2), (a3), and (a4) are for 2012; (b1), (b2), (b3), and (b4) are for 2013; (c1), (c2), (c3) and (c4) are for 2014; (d1), (d2), (d3), and (d4) are for 2015; (e1), (e2), (e3), (e4) and (f1) are for 2016.





895

896

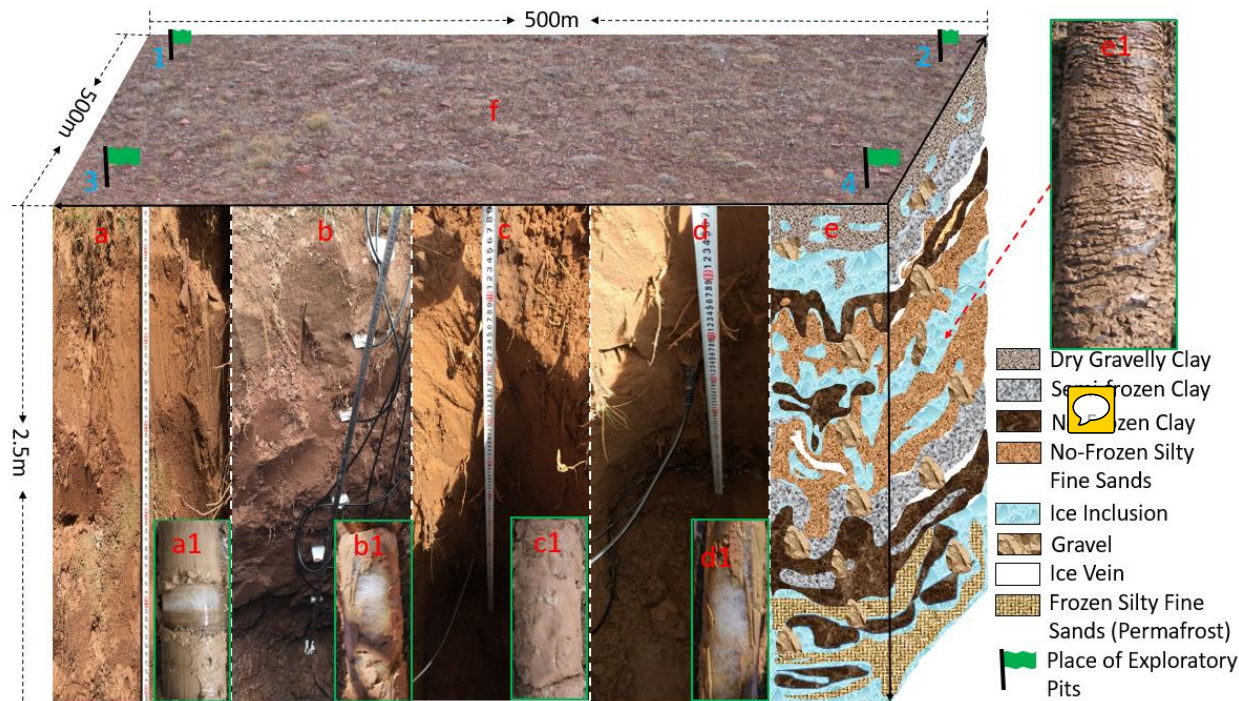
**Figure 5.** Regression comparison between observation and modeled methane fluxes with four different seasonal definitions and classification models. Panels (a), (b), (c), and (d) are for the SMT, JMC, VCT, and VPC methods, respectively.

897

898

899

900

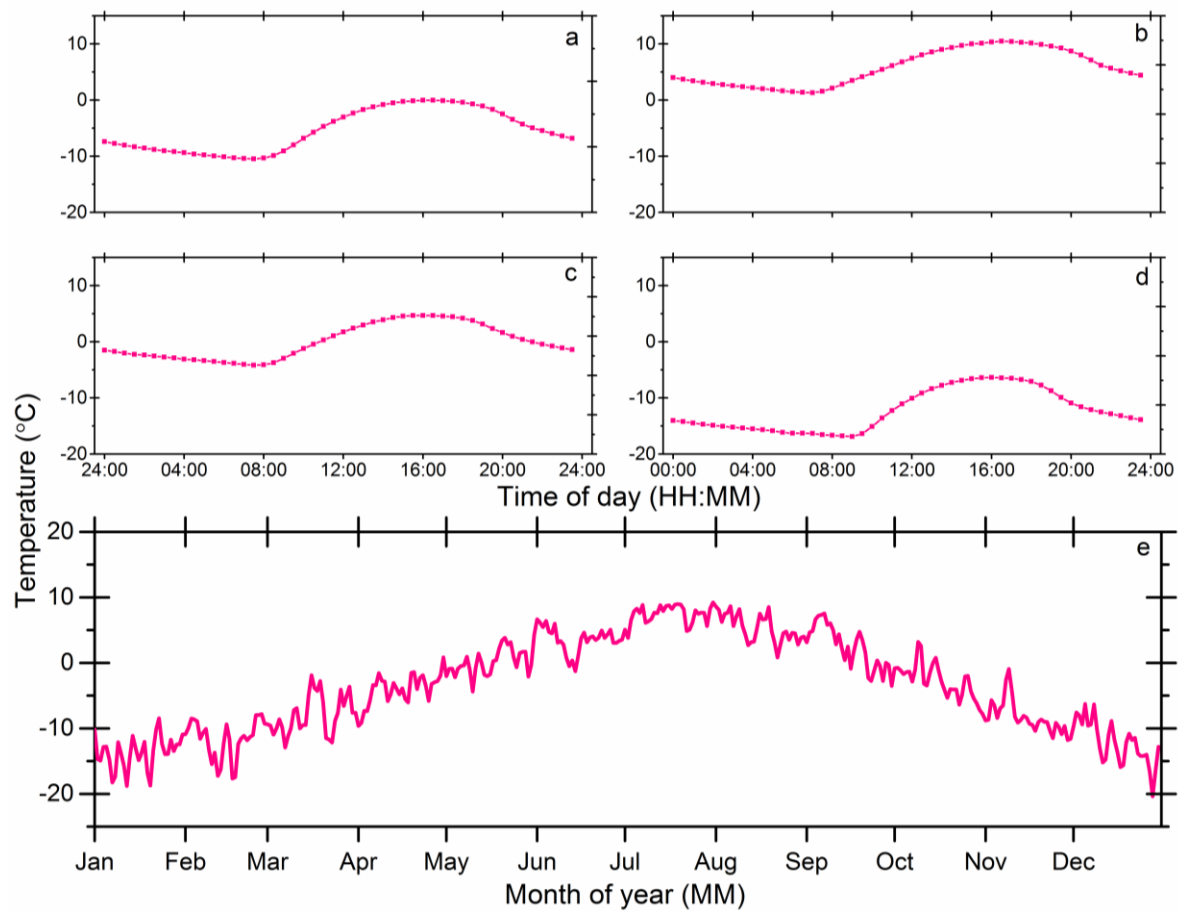


901 **Figure 6.** Location of exploratory pits and drillings in this study in autumn: (f) is photo of a typical ground surface (October 16th, 2014). Green flags  
 902 represent the location for the soil survey by test pitting and drilling. (a), (b), (c), and (d) are test pitting sections for active layer 0 – 250 cm depths  
 903 soil water content and temperature measured in eddy covariance North (1), South (2), East (3), and West (4) corners, respectively. (a1), (b1), (c1),  
 904 and (d1) are drilling cores, with clear ice (white) in (a1), (b1), and (d1), but not in (c1); (e) provides an illustration that combines results from  
 905 drillings, test pitting and multi-channel ground-penetrating radar (Malå Geoscience, Sweden) for active layer variations in permafrost area during the  
 906 autumn season; and (e1) is a core sample of the same drilling (October 16<sup>th</sup>, 2014).  
 907  
 908  
 909

910 **Supplement**911 **Supplementary Table 1** Seasonal soil water content (SWC, %) of winter<sub>=</sub>, spring<sub>=</sub>, summer<sub>=</sub>, and autumn<sub>=</sub> from 2012 to 2016.

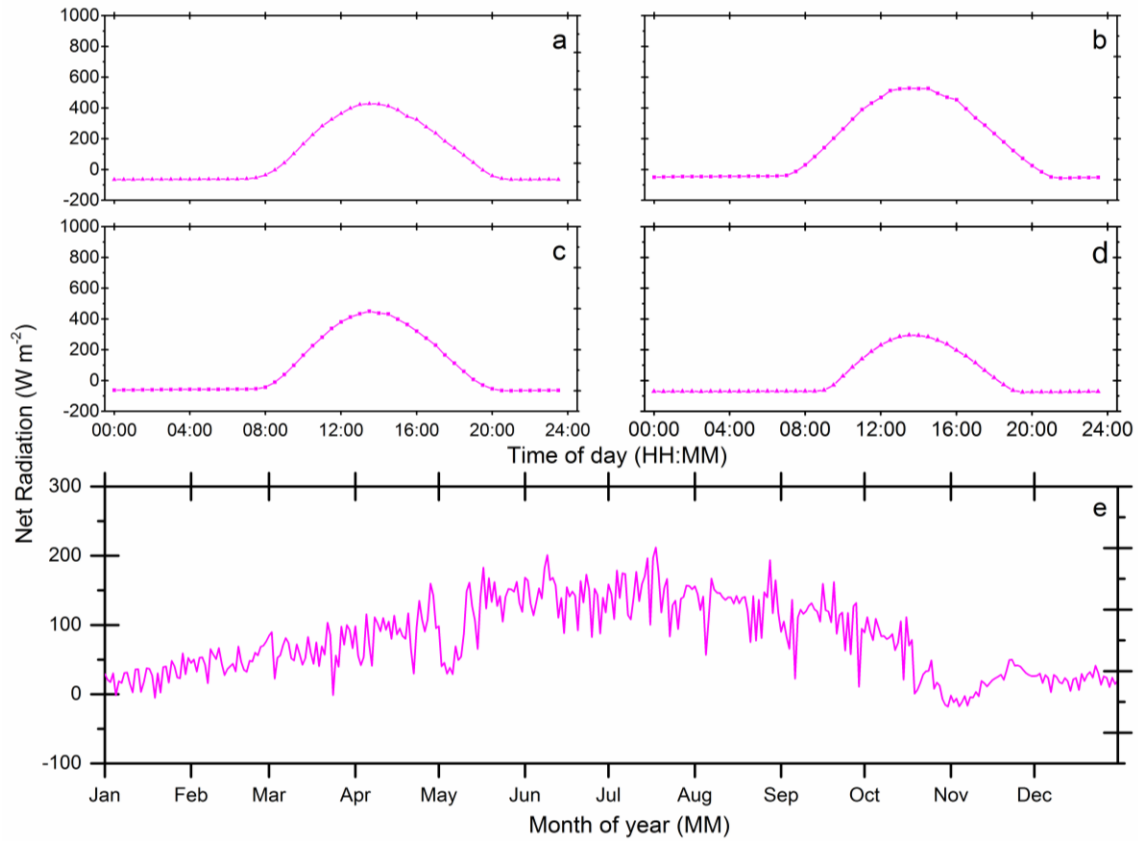
Seasonal	Period	10 cm	20 cm	40 cm	80cm	160cm
Soil Water Content (SWC), %						
Winter <sub>=</sub>	2012 early	0.11	0.08	0.07	0.11	0.14
	2012-2013	0.10	0.08	0.07	0.11	0.16
	2013-2014	0.10	0.08	0.07	0.11	0.13
	2014-2015	0.10	0.08	0.07	0.11	0.17
	2015-2016	0.10	0.08	0.07	0.11	0.16
	2016 later	0.10	0.08	0.07	0.12	0.19
	Average	0.10	0.08	0.07	0.11	0.16
Spring <sub>=</sub>	2012	0.13	0.09	0.08	0.11	0.13
	2013	0.12	0.09	0.08	0.11	0.13
	2014	0.12	0.08	0.07	0.11	0.13
	2015	0.13	0.09	0.08	0.11	0.14
	2016	0.12	0.09	0.08	0.13	0.15
	Average	0.12	0.08	0.08	0.11	0.14
Summer <sub>=</sub>	2012	0.18	0.11	0.10	0.17	0.27
	2013	0.16	0.11	0.11	0.19	0.25
	2014	0.16	0.10	0.10	0.16	0.24
	2015	0.16	0.10	0.10	0.19	0.28
	2016	0.16	0.10	0.09	0.18	0.28
	Average	0.17	0.10	0.10	0.18	0.26
Autumn <sub>=</sub>	2012	0.14	0.09	0.08	0.14	0.21
	2013	0.14	0.09	0.09	0.15	0.20
	2014	0.16	0.10	0.10	0.16	0.22
	2015	0.15	0.10	0.09	0.15	0.21
	2016	0.16	0.10	0.09	0.16	0.21
	Average	0.15	0.10	0.09	0.15	0.21

912



914

915 **Supplementary Figure 1.** Air temperature ( $T_{air}$ ) of 3 meters above the ground surface: (a), (b),  
 916 (c), and (d) are half-hour scale mean values in spring, summer, autumn, and winter, respectively;  
 917 (e) shows diel-scale mean values from 2012 to 2016.



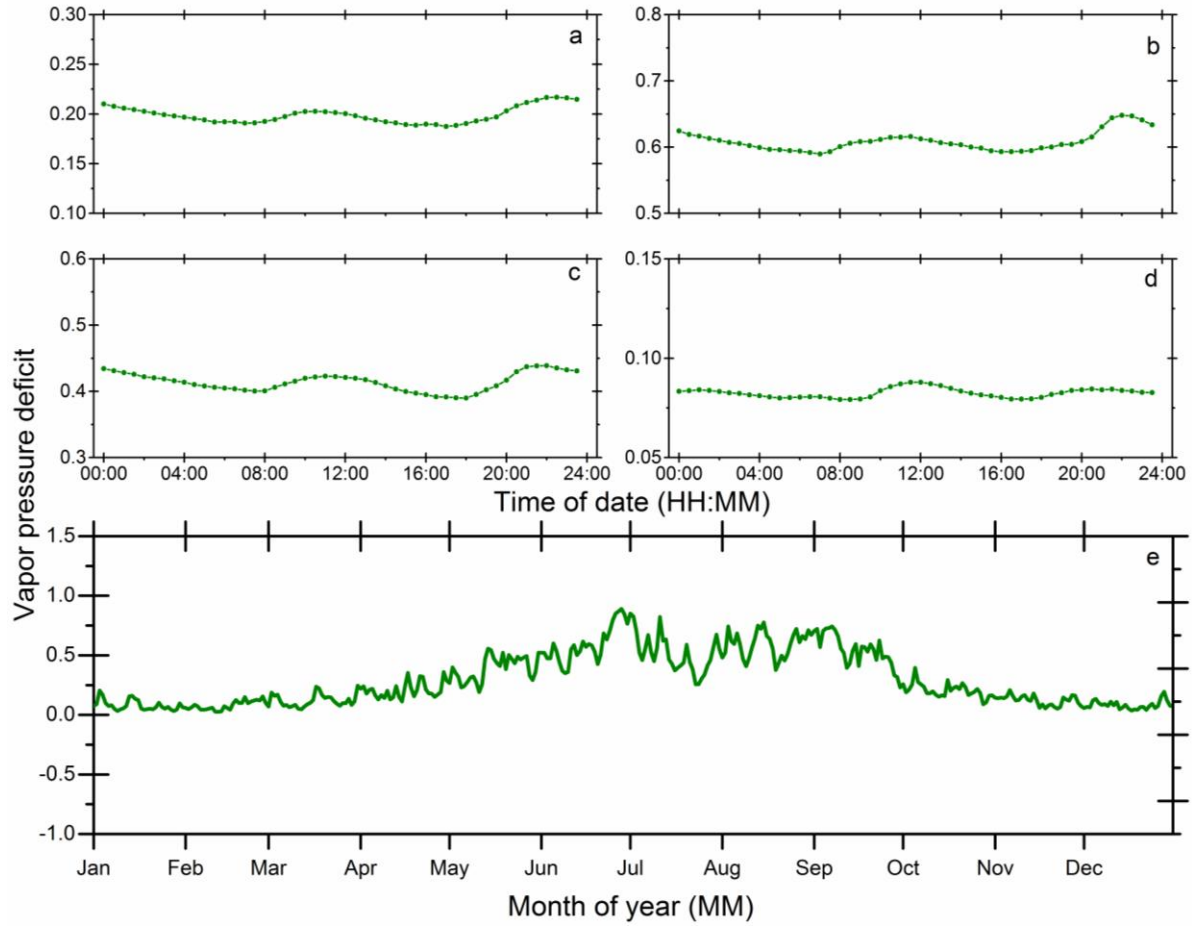
918

919 **Supplementary Figure 2.** Net radiation ( $R_n$ ) of 3 meters above the ground surface: (a), (b), (c),

920 and (d) are half-hour scale mean values in spring, summer, autumn, and winter, respectively; (e)

921 shows diel-scale mean values from 2012 to 2016.

922



923

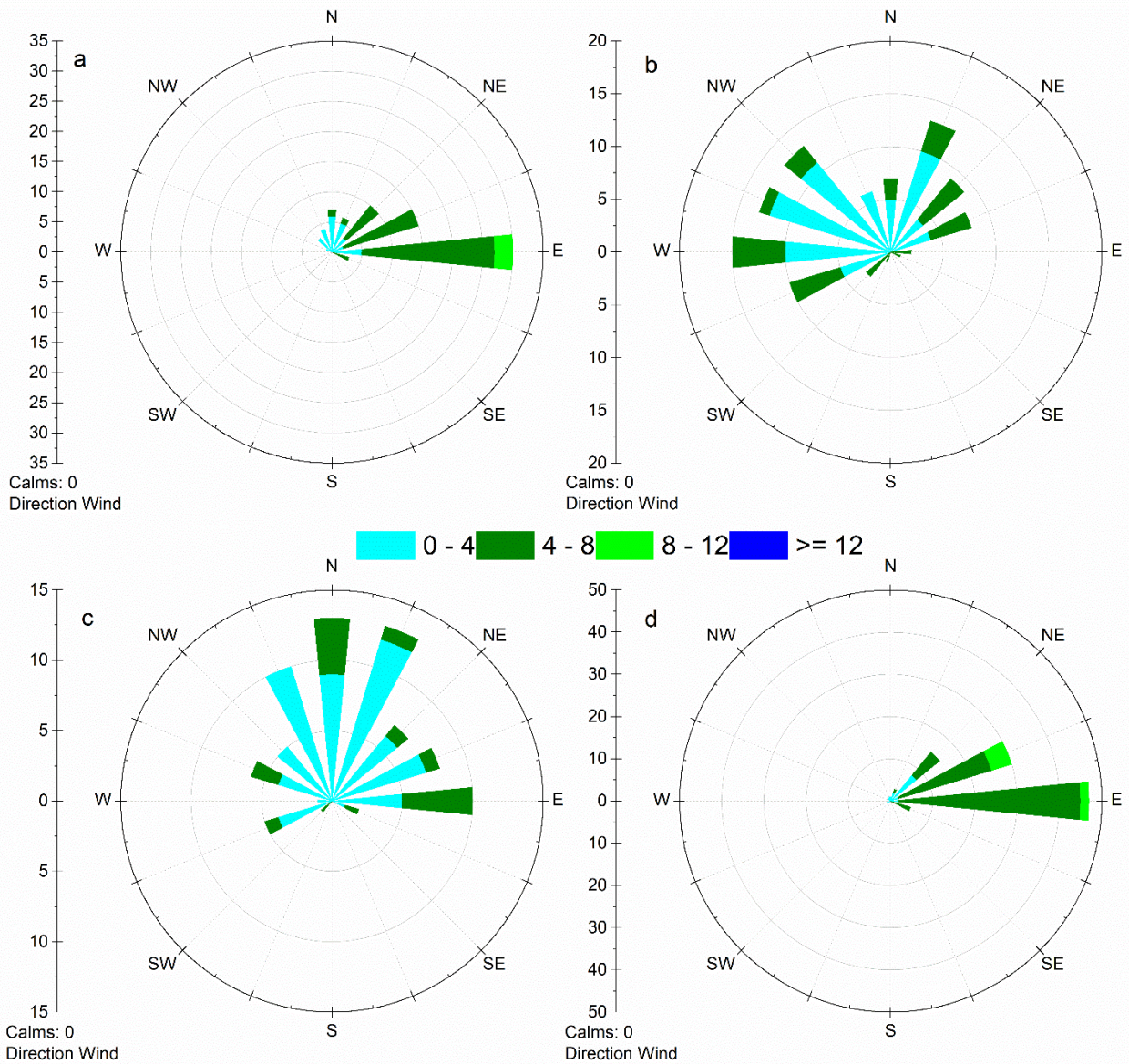
924 **Supplementary Figure 3.** Vapor pressure deficit (VPD) of 3 meters above the ground surface:

925 (a), (b), (c), and (d) are half-hour scale mean values in spring, summer, autumn, and winter,

926 respectively; (e) shows diel-scale mean values from 2012 to 2016.

927

928



929

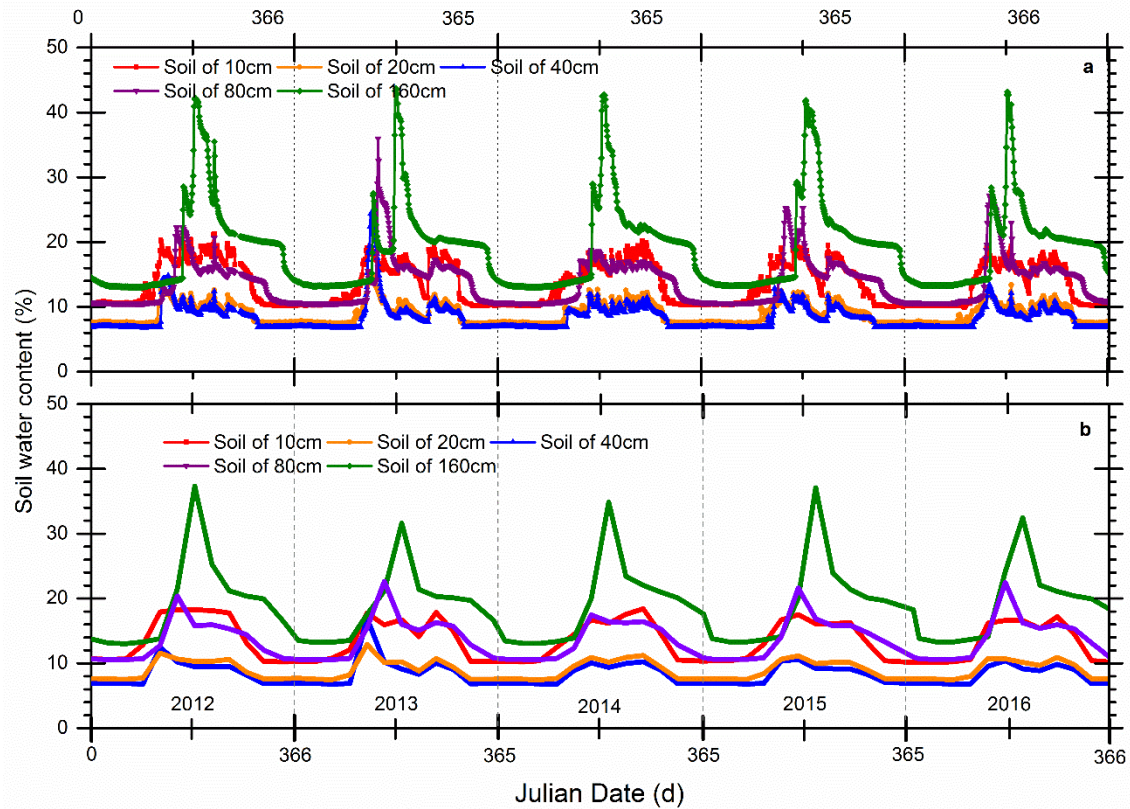
930 **Supplementary Figure 4.** Diel mean of wind speed and direction between 2012 and 2016. All

931 data are presented as mean values with standard deviations (mean  $\pm$  standard deviation).

932

933

934



935

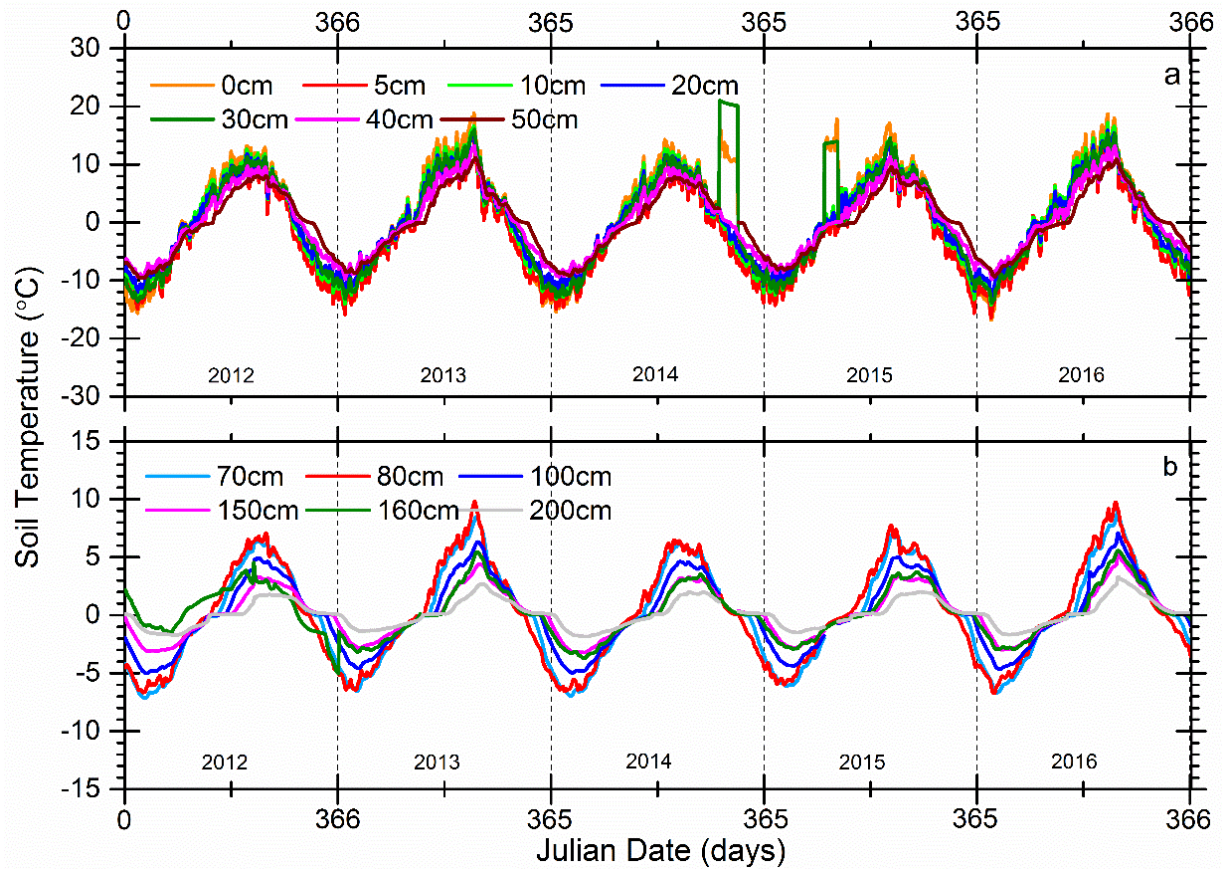
936 **Supplementary Figure 5.** Comparison between soil water content (SWC) of two different time

937 resolutions from 2012 to 2016, (a) is the half-hour scale SWC at soil depths of 10 cm, 20 cm, 40

938 cm, 80 cm, and 160 cm; and (b) is the 4-hour mean SWC for the same depths.

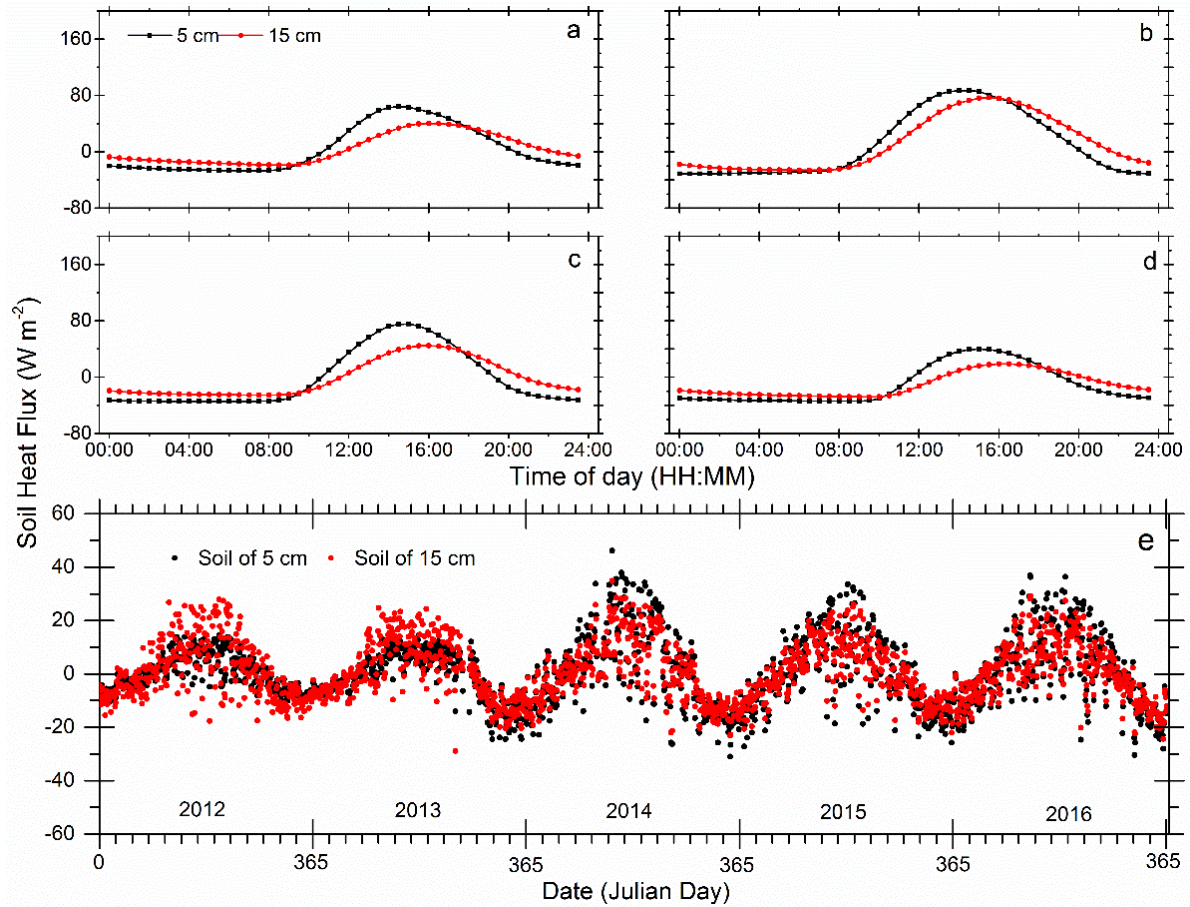
939





940

941 **Supplementary Figure 6.** Half-hour scale of 0 – 200 cm soil temperature ( $T_{soil}$ ) variations  
 942 from 2012 to 2016, (a) is for soil depths of 0 cm, 5 cm, 10 cm, 20 cm, 30 cm, 40 cm, 50 cm, (b)  
 943 is for soil depth of 70 cm, 80 cm, 100 cm, 150 cm, 160 cm, and 200 cm.



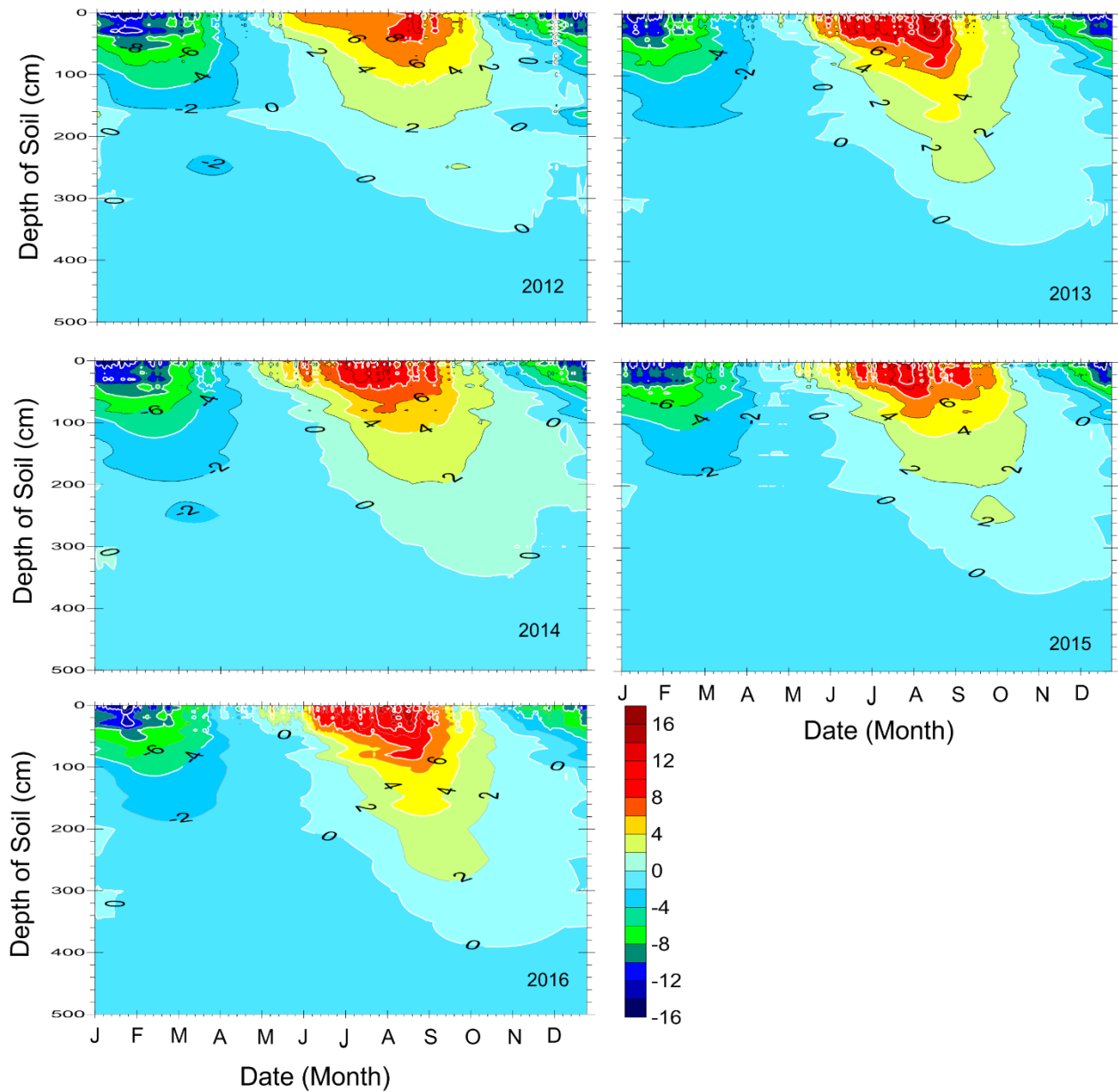
944

945 **Supplementary Figure 7.** Soil heat flux (SHF) at depth of 5 cm and 15 cm: (a), (b), (c), and (d)

946 are half-hour scale mean values in spring, summer, autumn, and winter, respectively; (e) shows

947 diel-scale mean values from 2012 to 2016.

948 .



949

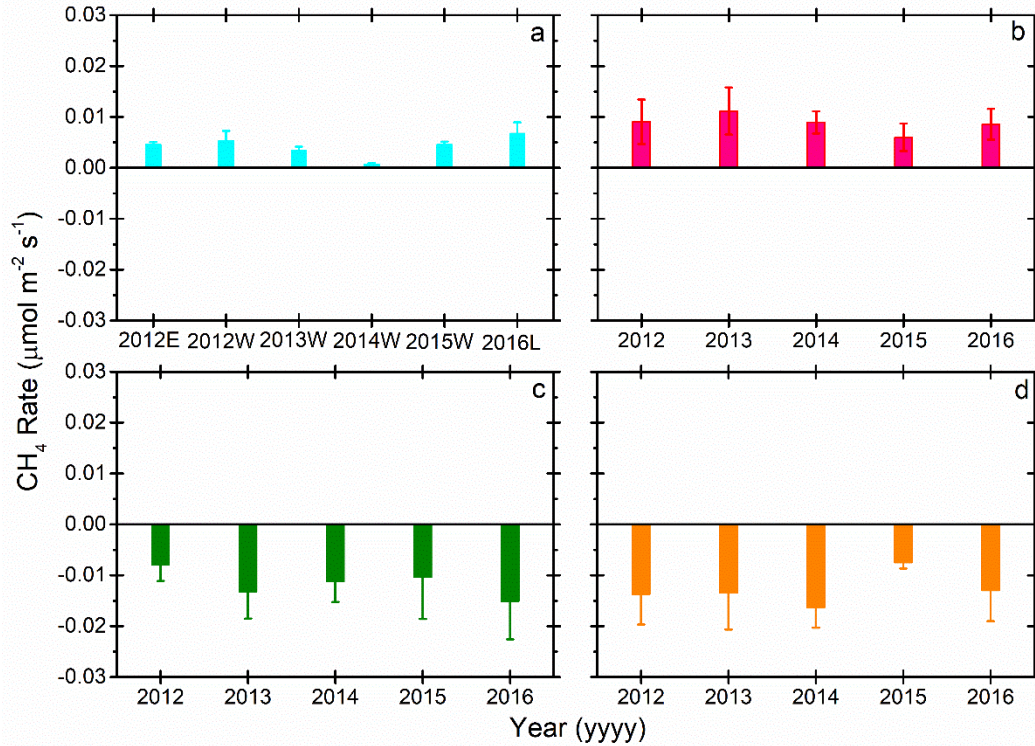
950 **Supplementary Figure 8.** Characteristics of the seasonal freezing and thawing processes of the

951 active layer for years: 2012, 2013, 2014, 2015, and 2016. Different colors represent the soil

952 temperature gradients from -16 °C to 20 °C. The depth of 0 °C represent the active layer

953 thickness (ALT).

954



955

956 **Supplementary Figure 9.** Seasonal CH<sub>4</sub> rate mean value from 2012 to 2016: (a) is winter, (b) is

957 spring, (c) is summer, and (d) is autumn. In the (a), 2012E is started from January 1<sup>st</sup>, 2012 and

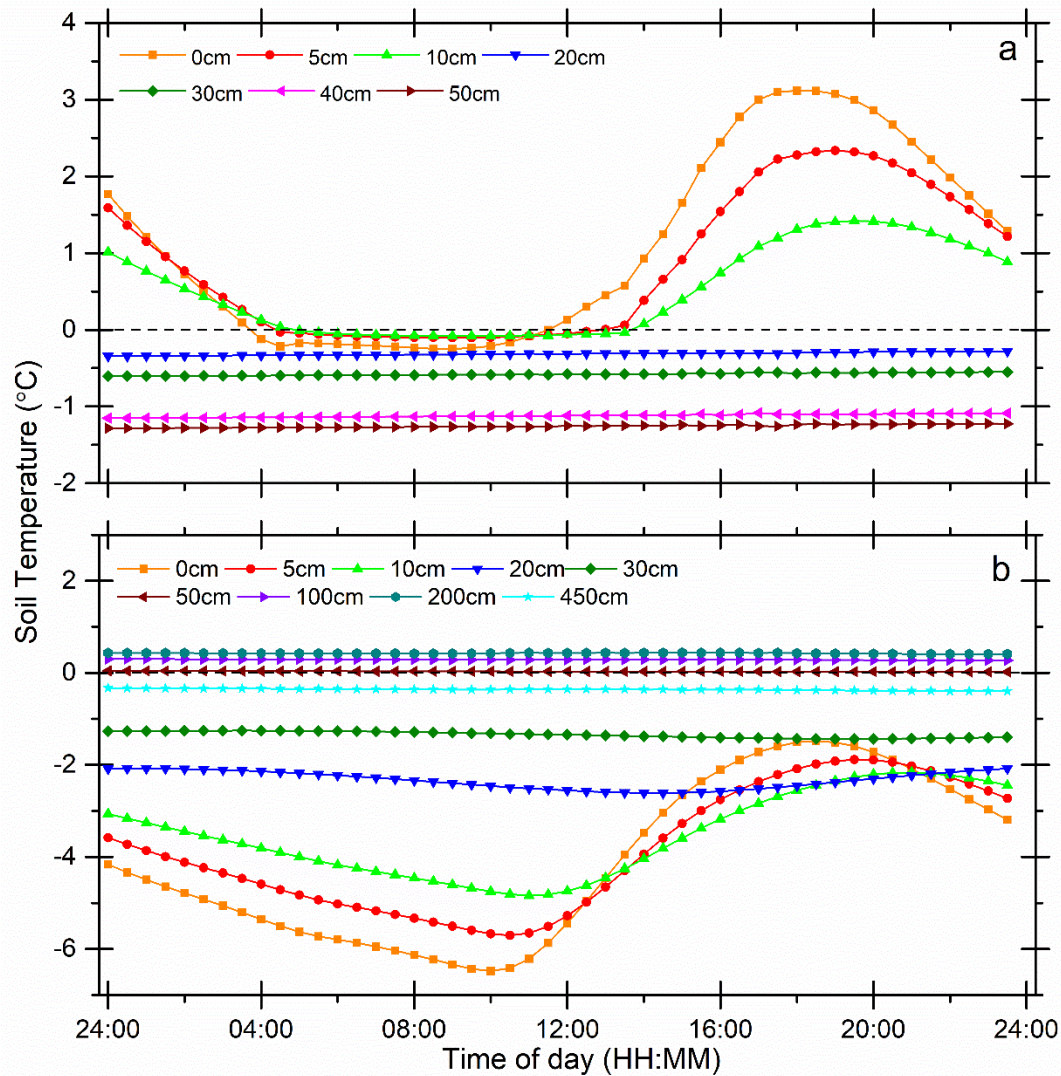
958 ended on February 17<sup>th</sup>, 2012; 2012W is started from 19<sup>th</sup> November, 2012 to 4<sup>th</sup> February, 2013;

959 2013W is started from 1<sup>st</sup> December, 2013 to 17<sup>th</sup> February, 2014; 2014W is started from 6<sup>th</sup>

960 November, 2014 to 4<sup>th</sup> February, 2015; 2015W is started from 9<sup>th</sup> November, 2015 to 15<sup>th</sup>

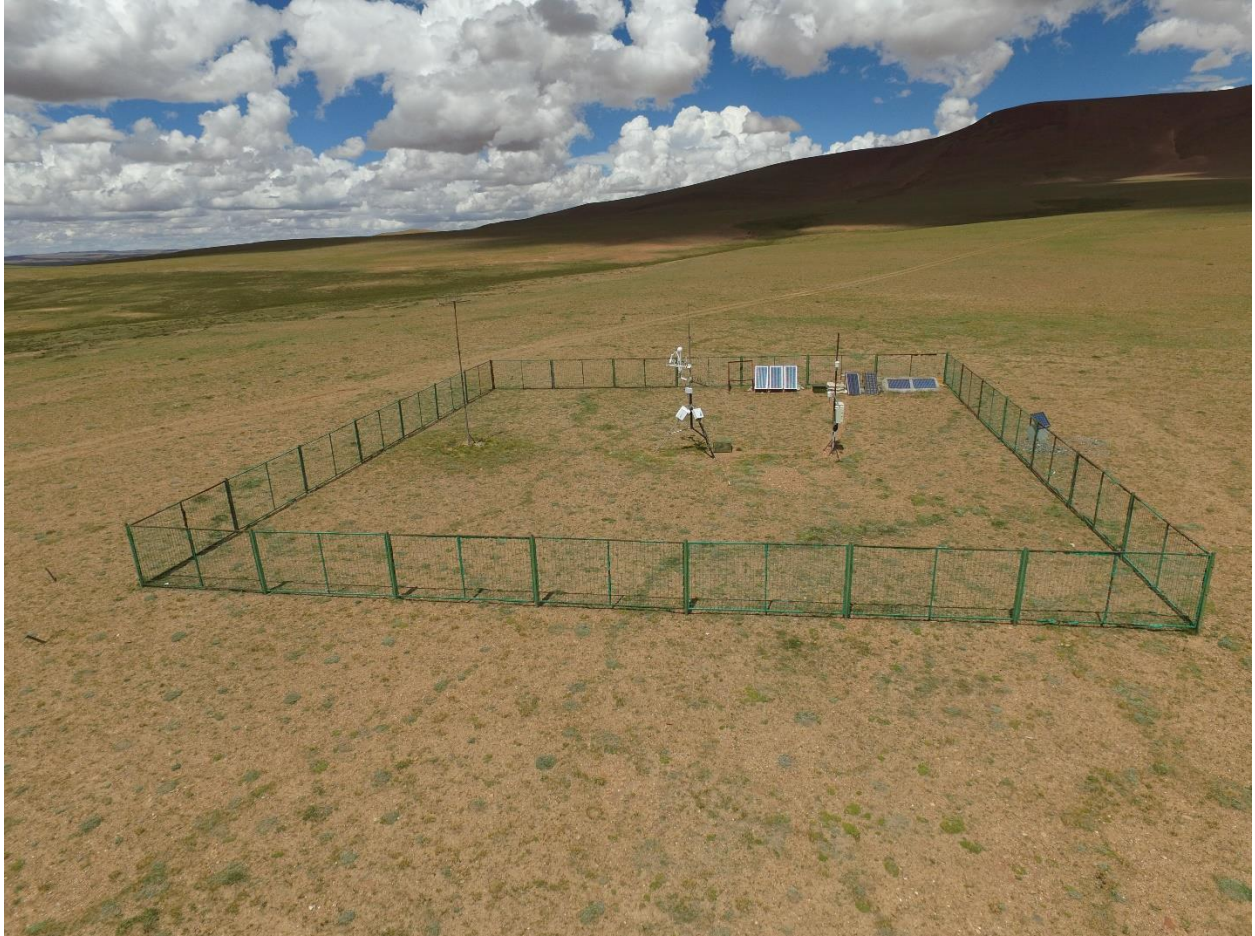
961 February, 2016; 2016L is started from October 26<sup>th</sup>, 2016 and ended on December 31<sup>st</sup>, 2016. All

962 data are presented as mean values with standard deviations (mean ± standard deviation).



963

964 **Supplementary Figure 10.** Average half-hour scale of 0 – 450 cm soil temperature (Tsoil) diel  
 965 variations from 2012 to 2016, (a) is for spring, (b) is for autumn. Notedly, during spring, the  
 966 Tsoil of 100cm, 200cm, 450cm were all below -2 °C and during autumn, the Tsoil of 40cm  
 967 almost overlap to Tsoil of 50cm, to make the figure more clearly, we removed the Tsoil of  
 968 100cm, 200cm, 450cm in figure (a) and removed the Tsoil of 40cm for figure (b).



969

970

**Supplementary Figure 11.** A bird's eye view of the eddy covariance in Beilu'he station